NASA TN D-1195

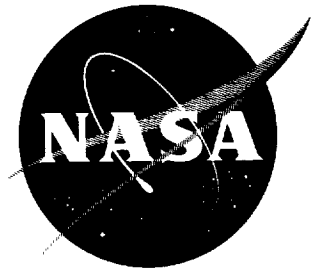

TECHNICAL NOTE

D-1195

INVESTIGATION OF CIRCULAR REINFORCEMENTS OF RECTANGULAR CROSS SECTION AROUND CENTRAL HOLES IN FLAT SHEETS UNDER BIAXIAL LOADS IN THE ELASTIC RANGE

By Albert Kaufman, Peter T. Bizon, and William C. Morgan

Lewis Research Center
Cleveland, Ohio

NATIONAL AERONAUTICS AND SPACE ADMINISTRATION
WASHINGTON

February 1962

NATIONAL AERONAUTICS AND SPACE ADMINISTRATION

TECHNICAL NOTE D-1195

INVESTIGATION OF CIRCULAR REINFORCEMENTS OF RECTANGULAR CROSS SECTION AROUND CENTRAL HOLES IN FLAT SHEETS UNDER BIAXIAL LOADS IN THE ELASTIC RANGE

By Albert Kaufman, Peter T. Bizon,
and William C. Morgan

SUMMARY

A study was made of the stress concentrations around holes in flat sheets reinforced with rings of rectangular cross section symmetrically mounted with respect to the sheets. The sheets were loaded in a biaxial loading machine, and stress-concentration factors for principal nominal stress ratios of 1:1, 1.5:1, 2:1, and 2.5:1 were determined. The sheet specimens were fabricated from plastic sheet and were instrumented with foil strain gages.

The best reinforcements reduced the stress-concentration factors to below 1.1 for the range of stress-field ratios studied. For a given hub thickness, increasing the ring diameter results in shifting the point of maximum effective stress from the inner rim of the hub to the sheet. If the ring diameter is kept constant, an increase in the hub thickness will shift the location of maximum stress or will have a negligible reinforcing effect. In most cases, increasing the thickness will raise the stresses in the sheet slightly.

The experimentally determined stress concentrations were compared with those calculated by a two-dimensional theoretical method proposed by L. Beskin. Although certain areas of disagreement were identified, the analytical method produced conservative results as far as the maximum stress-concentration factors were concerned when the outer diameter of the reinforcement was 1.7 times the hole diameter or greater.

INTRODUCTION

The presence of openings in missile or space-vehicle tanks requires special design consideration to ensure structural integrity. Stress concentrations resulting from openings conventionally are reduced by

increasing the material thickness locally. However, the manner in which the added material is distributed around the opening is of great importance in obtaining optimum reinforcement. In this report, the term "optimum reinforcement" implies a reinforcement geometry in which the maximum stress concentration, considering all locations, approaches unity as closely as possible. The best reinforcement of those tested will therefore be the one that is closest to an optimum reinforcement.

Various theoretical methods have been proposed for designing reinforcements (refs. 1 to 15), but relatively little experimental work has been done to determine their validity. In general, these analyses are two-dimensional, although in reference 2 an attempt is made to take into account localized bending due to a nozzle on one side of the plate. The two-dimensional assumption can lead to erroneous conclusions when large reinforcement thicknesses are involved. The flat-plate assumption is probably not too severe a restriction because, in most missile work, the diameter-to-thickness ratio of the tank components is very large, and the reinforcement area is relatively small. Differences exist, however, among the basic assumptions of references 1 to 15. Some assume that the reinforcement is concentrated at the rim of the hole; others assume that the reinforcement area is integral with the plate, and still others assume uniform shear on the contact surfaces between the reinforcing rings and the plate. Many of the analytical methods ignore the stress concentration in the plate at the outer edge of the reinforcement. On the basis of the literature, it appeared that the method proposed in reference 1 offered an approach commensurate with practical design because it allowed stress-concentration factors to be calculated at any location in the reinforcement area or plate and could take into account any stress-field ratio.

Experimentally, strains have been measured around reinforced openings in pressure vessels, as reported in references 16 to 18. These papers contain useful guides for reinforcing openings, but the experimental analyses were performed on relatively thick walled tanks and cannot be applied directly to the membrane-type walls used in space-vehicle applications. Some experimental work has been accomplished with reinforcements in flat plates, as reported in references 19 and 20, but the plates were loaded only in uniaxial tension, and the range of reinforcement sizes and proportions was limited.

An experimental investigation was undertaken at the Lewis Research Center to determine the applicability of the analytical method of reference 1 and also the best configurations under various biaxial stress fields. The research described herein employed flat sheets of a methyl methacrylate plastic having central holes reinforced with rings of rectangular cross section (see fig. 1). The reinforcing rings were cemented to each side of the sheet to produce a reinforcement hub symmetrical with respect to the plane of the sheet.

A range of hub diameters up to three times the hole diameter and of hub thicknesses up to 11 times the sheet thickness was studied. In this investigation the ratio of hole diameter to sheet thickness was kept constant. The 8:1 ratio chosen for this investigation probably represents the smallest ratio likely to be encountered for openings in missile and space vehicles and represents the largest practical departure from the plane stress condition. This is so because the hub stresses normal to the plane of the sheet will be reduced, as is discussed later in this report. Stress fields with principal stress ratios of 1:1, 1.5:1, 2:1, and 2.5:1 were imposed within the elastic range. Effective stress-concentration factors were calculated based upon the von Mises distortion-energy theory. Another phase of this program was to study tapered reinforcements; the results are reported in reference 21.

SYMBOLS

C location at midpoint of hub inner rim on x-axis (see fig. 1)

H location in sheet adjacent to hub on x-axis (see fig. 1)

K effective stress-concentration factor

O location in sheet adjacent to hub at some angle from y-axis (see fig. 1)

p uniform hydrostatic stress at infinity

q uniform shearing stress at infinity

V location in sheet adjacent to hub on y-axis (see fig. 1)

X ratio of outer diameter to inner diameter of hub

Z ratio of hub thickness to sheet thickness

Θ angle to location O as measured from y-axis (see fig. 1)

σ normal stress, psi

τ shear stress, psi

Subscripts:

C location C

exp experimental

H	location H
max	maximum
0	location 0
r	radial direction
th	theoretical
V	location V
x	direction of minimum nominal principal stress
y	direction of maximum nominal principal stress
z	direction normal to plane of sheet
θ	tangential direction
1	index for maximum nominal principal stress
2	index for minimum nominal principal stress
1r	first of duplicate back-to-back radial strain gages
2r	second of duplicate back-to-back radial strain gages
1θ	first of duplicate back-to-back tangential strain gages
2θ	second of duplicate back-to-back tangential strain gages

Superscripts:

–	maximum stress at given radius for uniform shear condition
*	stress at given radius for uniform hydrostatic condition

APPARATUS, SPECIMENS, AND EXPERIMENTAL PROCEDURE

Apparatus

The biaxial tensile testing machine shown in figure 2 was constructed to produce the required loading. It consisted of a rectangular metal frame with a bank of five hydraulic cylinders on each side. The cylinders on opposite sides were manifolded together to produce a uniform loading, but the vertical and horizontal banks were pressurized

from separate lines. The pressures were measured on Bourdon pressure gages having accuracies of 0.1 percent of full scale. By varying the pressures to the vertical and horizontal banks, different biaxial stress fields were imposed on the specimen.

Specimens

The specimens were rectangular sheets of a methyl methacrylate plastic approximately 16 by 18 inches and nominally 1/8 inch thick with 1-inch-diameter central holes. In order to distribute the load as evenly as possible, the specimens were pin-loaded through 10 holes on each side; that is, the piston of each hydraulic cylinder pulled on a pair of adjacent pins through a linkage system.

Reinforcing rings of the same plastic as the sheet material were cemented with cyanoacrylate adhesive on each side of the sheet around the hole. These rings were machined to the same thickness as the flat sheet to which they were applied, since there were variations in thickness between specimens. There were also thickness variations within individual specimens. Despite the most careful selection, the thickness at the edges varied as much as ±5 percent of the thickness at the center, where the average thickness always occurred. Some of the experimental error can be attributed to these thickness variations. For a specimen of a given hub diameter, the hub thickness was gradually built up by cementing additional rings on each side of the plate between tests. Tests on tensile specimens showed that the strain-gage cement had no effect on the mechanical properties of this plastic.

Experimental Procedure

Foil strain gages with 1/16-inch-square elements were mounted along the rim of the hole and back to back on the sheets at various points adjacent to the hub as shown in figure 1. The angle Θ, shown in figure 1, was based on the theoretical method of reference 1. Care was taken to put only 8 milliamperes of current through the strain gages to prevent damage because the plastic dissipates the heat slowly. The strain-gage output was recorded on an automatic multichannel recorder with an accuracy of ±1 percent.

The hydraulic cylinder pressures for various stress fields and the resulting nominal stresses were determined by testing a flat sheet with strain gages and no central hole. It was found that over a central area 3 inches square (a region that would cover the largest reinforcement ring used) the maximum strains at any point were within ±5 percent of the strains measured at the center of the plate; this held true under

all biaxial loading conditions. Farther from the center edge effects became more pronounced and the stresses became more nonuniform. Uniformity of the stresses in the ring section is shown in the photoelastic fringe patterns for each stress field in figure 3. Using the combinations of pressures calibrated for the stress-field ratios of 1:1, 1.5:1, 2:1, and 2.5:1, a flat unreinforced specimen with strain gages around the rim of the central hole was tested. The experimentally determined maximum stress concentrations were about 3 percent less than those predicted theoretically, as shown in table I for the case $X = 1$, $Z = 1$.

The specimen initially had one ring cemented on each side and had strain gages mounted as in figure 1. In imposing the various biaxial stress fields, the horizontal load was constant and the vertical load was varied. The specimen was loaded by uniformly and simultaneously bringing it up to the previously determined combination of vertical and horizontal loads. For each configuration, four different combinations of loads were imposed and the values for the stress-field ratios of 1:1, 1.5:1, 2:1, and 2.5:1 were determined by interpolation. After each loading, the specimen was unloaded and strain readings were taken to determine the zero drift before proceeding to the next loading. This process was repeated a second time for each configuration. As mentioned before, the load and no-load times were equal. The strain data were then entered into a computer program which corrected for zero drift, computed the best straight line through the data by means of the method of least mean squares, checked the linearity of the data, and determined the strains, stresses, and effective stress-concentraction factors for the 1:1, 1.5:1, 2:1, and 2.5:1 stress-field ratios for locations C, V, H, and O.

The hub thickness was built up by cementing on each side another ring with the same thickness as the sheet, and the test was repeated. This procedure was followed until the hub thickness was built up to 11 times the sheet thickness. The hub was then milled down to the original set of rings. At this point the normal and tangential strain gages at C (C_Z and C_θ of fig. 1) were removed, and another set of gages was mounted with the positions reversed to obtain a second set of readings at location C. The process of testing and building up the hub was then repeated. The results were averaged with the first series of tests. Reinforcement rings 1.4, 1.7, 2.0, 2.5, and 3.0 inches in outer diameter were investigated in this way.

ANALYTICAL PROCEDURE

Experimental results were compared with computations of stress-concentration factors obtained from equations in reference 1 and tabulated in table I. Using conventional two-dimensional theory of elasticity, effective stresses were computed based on the von Mises distortion

energy theory. Using these, stress-concentration factors were computed for reinforcement rings around holes in sheets under biaxial loads. The biaxial loading conditions examined were for 1:1 and 1:-1 stress-field ratios corresponding to conditions of hydrostatic stress and pure shearing stress, respectively. Other types of biaxial loading can be obtained by superposition of these two conditions.

If p is the principal stress at infinity for the 1:1 stress field, q is the principal stress at infinity for the 1:-1 stress field, and $(p + q)/(p - q)$ equals the desired ratio of maximum to minimum principal stresses, then

(1) For a 1:1 stress-field ratio, $\frac{p + q}{p - q} = 1$, and $q = 0$.

(2) For a 1.5:1 stress-field ratio, $\frac{p + q}{p - q} = 1.5$, and $p = 5q$.

(3) For a 2:1 stress-field ratio, $\frac{p + q}{p - q} = 2$, and $p = 3q$.

(4) For a 2.5:1 stress-field ratio, $\frac{p + q}{p - q} = 2.5$, and $p = (7/3)q$.

The effective stress-concentration factor for location V, H, or O based on distortion energy theory is

$$K = \sqrt{\frac{\sigma_r^2 + \sigma_\theta^2 - \sigma_r\sigma_\theta + 3\tau_{r\theta}^2}{p^2 + 3q^2}}$$

where σ_r is the radial stress, σ_θ is the tangential stress, and $\tau_{r\theta}$ is the shear stress in the biaxially loaded sheet. In the case of location C, σ_r will be replaced in the equation by σ_z, the stress normal to the plane of the sheet. Since locations C, V, and H (fig. 1) lie along axes of symmetry, the shear stresses will be zero for these positions. For location O not on these axes, the shear stress must be calculated. This method was programmed for an IBM 704 computer.

It can be shown, using a circular reinforcement of constant cross section around a hole, that the maximum stress concentration occurs at location C, where the direction of the maximum nominal principal stress is tangent to the hole rim. From Beskin's method the maximum effective stress-concentration factor in the sheet adjacent to the hub will occur either at location V or H, or at an angle Θ such that

$$\cos 2\Theta = -\frac{\bar{\sigma}_r^*\bar{\sigma}_r + \bar{\sigma}_\theta^*\bar{\sigma}_\theta - \frac{\bar{\sigma}_r^*\bar{\sigma}_\theta + \bar{\sigma}_\theta^*\bar{\sigma}_r}{2}}{\bar{\sigma}_r^2 + \bar{\sigma}_\theta^2 - \bar{\sigma}_r\bar{\sigma}_\theta - 3\bar{\tau}_{r\theta}^2}$$

where $\overline{\sigma}_r$, $\overline{\sigma}_\theta$, and $\overline{\tau}_{r\theta}$ are the solutions for the maximum radial, tangential, and shear stresses in the sheet for a 1:-1 stress-field ratio of magnitude q, and σ_r^* and σ_θ^* are the solutions for a 1:1 stress-field ratio of magnitude p. These stresses can be readily determined from reference 1. The angle Θ will vary as X or Z or the stress field is changed. For example, for the X = 1.7 reinforcement, Θ will vary from 45.28° to 37.18° over the range of thicknesses to be studied and for stress-field ratios of 1.5:1, 2:1, and 2.5:1, the average value being 42°. At X = 2, Θ varies from 42.88° to 28.32° with an average of 38°; at X = 2.5, Θ is 39.28° to 12.31° with a 34.5° average; and Θ varies from 36.00° to 15.04° with an average of 30° for X = 3. Because of physical limitations, these average values of Θ were used in the experimental work.

RESULTS AND DISCUSSION

The results of the biaxial tensile tests are shown in table I. Both experimental and theoretical stress-concentration factors are indicated for locations C, V, H, and O for each configuration at each stress-field ratio. As pointed out previously, in the case of location O, a compromise had to be made for placing the strain gages. The last column in table I shows the theoretical stress-concentration factor for the critical location for each condition. The second last column shows the theoretical stress-concentration factor for the actual location O in the test specimen. By comparing these two columns, it is evident that the displacement of gages at location O from their critical position had only a slight effect on the theoretical values.

Verification of Theoretical Method of Locating Strain Gages in Sheet

On one of the configurations (X = 1.4, Z = 11) strain-gage rosettes were mounted on the sheet along the outer rim of the reinforcement at angles Θ of 0°, 30°, 45°, 60°, and 90°. A number of separate tests were necessary to accomplish this program, since there was not enough space to mount all the strain gages at the same time. The measured distribution is shown in figure 4.

The experimental effective stress-concentration factors for the 1:1 stress-field ratio varied from 0.93 to 1.04 with an average value of 0.99. If this had been a perfect hydrostatic field, the values would have been identical at every point along the circumference. The nonuniformity of the stress field had more effect on the measurements at location O than on those taken elsewhere because none of the gages at O were duplicated as they were for the measurements at locations V and H. This factor probably accounted for much of the scatter of the experimental data for the 1:1 stress field in figure 4.

The peaks of the experimental curves for the 1.5:1, 2:1, and 2.5:1 stress fields occurred at about 45°. Actually the curves are so flat that an error of even 10° would make no appreciable difference in the stress-concentration factor. The important point indicated in figure 4 is that these peaks occurred at approximately the same angle as those of the theoretical curves. On the basis of this agreement, it was decided that in all other cases the strain-gage rosette would be located as closely as possible to the angle predicted by Beskin's method. One of the notable observations derived from figure 4 is that the experimental stress-concentration factors were considerably smaller than the theoretical values. As is shown later, this conclusion was generally true for location O for every configuration. The discrepancy was particularly noticeable in this case because the departure from the plane-stress assumption was most pronounced in this configuration as a result of the combination of small outer diameter and large hub thickness.

Effect of Stress-Field Ratio on Experimental Stress-Concentration Factors at Locations C and O

In figure 5 experimental stress-concentration factors for locations C and O are plotted against stress-field ratios. Location O was chosen rather than V or H because the maximum stress concentration in the sheet occurred there in most cases.

The theoretical curve for the stress-concentration factor at C for an unreinforced hole is also shown in figures 5(a) to (e). It can be seen that the minimum reinforcement (X = 1.4, Z = 3 in fig. 5(a)) considerably improved the specimen.

The effect of increasing the stress-field ratio was an increase in the stress-concentration factors at both C and O. This change was most significant at location C in going from a 1:1 stress field to a more nonuniform one when the hub thickness was small. The stress-concentration factors at both locations C and O were not much worse for a 2.5:1 stress-field ratio than for a 2:1 stress-field ratio.

Magnitude and Location of Maximum Stress-Concentration Factors in Hub and Sheet

In figure 6 the stress-concentration factor is plotted against the parameter X for the 1:1, 1.5:1, 2:1, and 2.5:1 stress-field ratios.

At the top of the figure the curves for location C are shown, while at the bottom the maximum measured stress-concentration factor in the sheet is plotted. The intersections of these sets of curves are shown to indicate where the highest stress concentration shifts from the reinforcement to the sheet. This maximum in the sheet usually occurred at location O, sometimes at V, and never at H within the range of geometries studied. All curves in figure 6 are extrapolated to the theoretical values for an unreinforced hole at $X = 1$.

In figure 6(a) (for $Z = 3$), the maximum stress concentration in the sheet always occurred at location O. Figure 6(b) (for $Z = 5$) also shows the maximum in the sheet occurring at location O, except for $X = 2.5$ for a 1.5:1 stress-field ratio, where it was at location V. In figures 6(c) and (d) (for $Z = 7$ and 9) the worst location was at V for $X = 1.7$ at a 1.5:1 stress-field ratio. The $Z = 11$ hub of figure 6(e) showed more cases in the region between $X = 1.7$ and $X = 2.5$, where the highest stress concentration in the sheet occurred at location V.

Selection of Reinforcement Geometry

Three-dimensional figures were constructed by plotting K_{max} (whether at location C or in the sheet) against both the X and Z parameters (fig. 7). The trend of the stress-concentration-factor curves for location C is an initial rapid decrease with increasing X and then a leveling off as X is increased further. The trend of the maximum stress-concentration factor curves in the sheet for values of X larger than 1.7 is to increase slightly with increasing values of X and in some cases to level out. Except for cases involving low values of Z, these two types of curves (K_c and K_{max} in the sheet) generally intersect between values of X of 1.6 and 1.8. The intersection of these two sets of curves is shown in figure 7 for each stress field. The dark shaded area is the location of the maximum stress-concentration factor in the sheet. For a given hub diameter, the effect of increasing the thickness is very small as far as the stress concentrations in the sheet are concerned; usually there is a slight increase in the stress-concentration factor. In each part of figure 7 the dark area is relatively flat because of this insensitivity of the stress-concentration factors in the sheet to changes in X and Z in that region.

The best reinforcements for each stress field therefore lie on the dark shaded surface near the intersection with the steep surface.

In figure 7(a) (for a 1:1 stress field) the dark area extends approximately from $X = 1.6$ and $Z = 2.9$. The maximum stress-concentration factor on this surface varies between 0.96 and 1.06. The best configurations for this stress-field ratio were $X = 1.7$ with Z between 5 and 11. The three-dimensional plot of the 1.5:1 stress-field ratio is shown in figure 7(b). The dark surface extends from $X = 1.7$ and

$Z = 3.5$ with K_{max} varying between 1.03 and 1.22. The best configurations are again $X = 1.7$ with Z from 5 to 11. Figure 7(c) (for the 2:1 stress-field ratio) shows the dark surface to be beyond $X = 1.7$ and $Z = 4.0$ with K_{max} from 1.05 to 1.25. The best configuration in this region was $X = 1.7$ and $Z = 11$. In figure 7(d) (for the 2.5:1 stress-field ratio) the boundary limits are about the same as for figure 7(c). The maximum stress-concentration factor on the dark surface varies from about 1.08 to 1.27, and again the best configuration is $X = 1.7$ and $Z = 11$.

Comparison of Experimental and Theoretical Stress-Concentration Factors

The ratios of the experimental to theoretical stress-concentration factors are plotted in figure 5 for locations C and O. For location C, there was better agreement as the stress-field ratio became larger.

As the hub thickness was increased, the ratio of experimental to theoretical stress-concentration factor for location C increased, while for location O it decreased. This trend occurred with all values of X, except for $X = 3.0$ in figure 5(c). In that case there was an initial decrease in the ratio of experimental to theoretical stress-concentration factor for location C as the hub was built up; however, as the hub was increased further, the ratio decreased again. The ratio of the maximum experimental to the maximum theoretical stress-concentration factor is shown in figure 8 for each configuration for the 1:1, 1.5:1, 2:1, and 2.5:1 stress-field ratios. Only the magnitudes of the maximum factors were considered; the locations of the experimental and theoretical highest stress concentrations were not necessarily the same.

A number of conclusions can be drawn from figure 8. The first is that, if Z is 3 or less, there is very good agreement between the experimental results and the method of reference 1. This is to be expected, since in this range the reinforcement approaches most closely the plane-stress condition assumed in the theoretical analysis. Also, when X is 1.7 or larger, Beskin's method is either in good agreement or on the conservative side. The worse discrepancy between the maximum experimental and theoretical stress-concentration factors was 27 percent in this range. Figure 8 shows that Beskin's method should never be used with values of Z greater than 3 when X is less than 1.7.

Comparison of Experimental and Theoretical Locations of Maximum Stress Concentration

The locations of the maximum stress concentrations, both theoretical and experimental, are shown in table II. This table shows whether the highest measured stress concentration occurred at the hub or in the sheet; if in the sheet, the angle Θ that was used is given. In addition to the highest experimental value, the theoretical value at the most critical experimental location and the highest theoretical value with its location are given.

It should be noted that the method of reference 1 was not always successful in predicting where the maximum stress concentration would occur. For example, there were 10 cases (most of them at 1.5:1 stress fields in the region between $X = 1.7$ and $X = 2.5$) where the maximum stress concentration occurred at V rather than at the theoretically predicted location O. There were also a few cases where the critical location in the sheet should theoretically have been at V but actually occurred at O. However, an examination of table I shows that for most of the cases where discrepancies occurred, K_V and K_O were nearly equal, so that the choice of critical location could be at either V or O within the experimental error. The tendency at large hub thicknesses and low stress-field ratios for the critical location to drift toward V seems well established, however, and agrees with Beskin in this manner.

Accuracy of Data

An indication of the accuracy of the experimental work can be obtained by comparing the stress-concentration factors at locations V, O, and H in table I for a 1:1 stress-field ratio. These factors should be equal. In the worst cases there was approximately a ± 5 percent spread among K_O, K_V, and K_H. It should be remembered, however, that the K_V and K_H values are the results of averaging symmetrically placed gages, whereas there were no symmetrical gages at O because of space limitations. Thus K_O is inherently less dependable than the other experimental values.

The accuracy of the method of measuring the experimental stress-concentration factors at C can be estimated by comparing the experimental and theoretical values in table I for an unreinforced hole ($X = 1$, $Z = 1$). The discrepancy in this case was between 2 and 3 percent for the various stress-field ratios.

Three-Dimensional Effects

Since the reinforcements are essentially cylinders with narrow bands of radial load, bending moments of varying magnitudes are induced that result in stresses normal to the plane of the sheet. Since these stresses are compressive at the inner rim of the reinforcement, they tend to produce an effective stress-concentration factor at this location measurably larger than that predicted by reference 1. However, since the reinforcement material is not as effective as assumed in the two-dimensional analysis, the effective stress-concentration factor in the sheet is smaller than that predicted by reference 1.

The relative magnitudes of these compressive stresses can be seen in figure 9. Varying X only, the magnitude of the ratio of the bending stress to the tangential stress at C, $(\sigma_z/\sigma_\theta)_C$, decreases as X increases. Varying Z only, the magnitude of this ratio generally decreases with decreasing Z. Thus, any change to a geometry that tends to satisfy the basic two-dimensional assumptions more closely generally decreases the bending stress in the reinforcement. Varying the stress-field ratio only, $(\sigma_z/\sigma_\theta)_C$ decreases with increasing stress-field ratio.

The 8:1 ratio of hole diameter to sheet thickness used in the test specimens in this investigation is lower than any that would normally be encountered in missile or space-vehicle applications. Any increase in this ratio will change the geometry in such a way that it will more closely approximate the two-dimensional assumptions of reference 1 for any given X and Z. Such an increase will be accompanied by a decrease in the bending stresses in the hub, and the maximum effective stress-concentration factors will agree more closely with those computed from reference 1.

CONCLUSIONS

The following conclusions may be drawn from the investigation of the reinforcing effect of rings of rectangular cross section around central holes in biaxially loaded flat sheets:

1. The best reinforcements for the 8:1 ratio of hole diameter to sheet thickness reduce the maximum stress-concentration factors to 1.1 or less over the range of stress-field ratios that was studied.

2. For thin-walled reinforcements, the highest stress is at the inner rim of the hub. For a large ratio of hub to hole diameter X, the critical location is generally in the sheet adjacent to the hub. As the hub diameter is further increased, the stresses in the sheet tend to get somewhat higher.

3. For configurations where the hub thickness is three times the sheet thickness or less, the two-dimensional method of Beskin gives good agreement with the experimental values at the inner rim of the hub. For all configurations and stress-field ratios, the maximum stress concentration in the sheet either agrees fairly well or is less than that predicted from Beskin's method. For all configurations with $X = 1.7$ or greater, Beskin's method is conservative at the location where the maximum effective stress occurs.

4. The effect of the hub thickness on the stress concentration at the inner rim is large, especially as the hub is initially built up. When the maximum effective stress is in the sheet, the effect on the stress concentration of increasing hub thickness is relatively small.

5. The effect of increasing the nominal principal stress-field ratio on a given configuration is an increase in the stress-concentration factor.

6. Although the experimental investigation was done only for an 8:1 ratio of hole diameter to sheet thickness, the larger ratios that are normally encountered in space-vehicle applications should result in closer agreement with the predictions from Beskin.

Lewis Research Center
National Aeronautics and Space Administration
Cleveland, Ohio, November 30, 1961

REFERENCES

1. Beskin, L.: Strengthening of Circular Holes in Plates Under Edge Loads. Jour. Appl. Mech., vol. 11, no. 3, Sept. 1944, pp. A-140-A-148.

2. Waters, E. O.: Theoretical Stresses Near a Circular Opening in a Flat Plate, Reinforced with a Cylindrical Outlet. Paper 58-A-171, ASME, 1958.

3. Nomura, Y.: On the Stiffening of the Edge of the Hole in an Orthogonally Aeolotropic Plate with a Circular Hole. Bull. Japan Soc. Mech. Eng., vol. 2, no. 6, May 1959, pp. 277-285.

4. Gurney, C.: An Analysis of the Stresses in a Flat Plate with a Reinforced Circular Hole Under Edge Forces. R. & M. 1834, British ARC, Feb. 24, 1938.

5. Mansfield, E. H.: Neutral Holes in Plane Sheet: Reinforced Holes Which are Elastically Equivalent to the Uncut Sheet. R. & M. 2815, British ARC, Sept. 1950.

6. Mansfield, E. H.: Stress Considerations in the Design of Pressurized Shells. CP 217, British ARC, Apr. 1955.

7. Mansfield, E. H.: Optimum Designs for Reinforced Circular Holes. CP 239, British ARC, 1956.

8. Hodge, P. G., Jr., and Perrone, Nicholas: Yield Loads of Slabs with Reinforced Cutouts. Jour. Appl. Mech., vol. 24, no. 1, Mar. 1957, pp. 85-92.

9. Weiss, H. J., Prager, W., and Hodge, P. G., Jr.: Limit Design of a Full Reinforcement for a Circular Cutout in a Uniform Slab. Jour. Appl. Mech., vol. 19, no. 3, Sept. 1952, pp. 397-401.

10. Hicks, R.: The Plane Stress Distribution in a Plate Containing a Reinforced Elliptical Hole. Street 1708, British ARC, Apr. 26, 1954.

11. Hicks, R.: The Design of Reinforced Elliptical Holes in Pressure Vessels. British Welding Jour., vol. 5, no. 3, Mar. 1958, pp. 130-132.

12. Reissner, H., and Morduchow, M.: Reinforced Circular Cutouts in Plane Sheets. NACA TN 1852, 1949.

13. Sezawa, K., and Kubo, K.: Stresses in a Plate with a Flanged Circular Hole. Rep. 84, Tokyo Imperial Univ., Aero. Res. Inst., vol. 7, no. 3, Sept. 1932, pp. 65-114.

14. Levin, E.: Elastic Equilibrium of a Plate with a Reinforced Elliptical Hole. Paper 59-A-45, ASME, 1959.

15. Levy, Samuel, McPherson, A. E., and Smith, F. C.: Reinforcement of a Small Circular Hole in a Plane Sheet Under Tension. Jour. Appl. Mech., vol. 15, no. 2, June 1948, pp. 160-168.

16. Taylor, J. Hall, and Waters, Everett O.: The Effect of Openings in Pressure Vessels. Trans. ASME, vol. 56, no. 3, Mar. 1934, pp. 119-140.

17. Schoessow, G. J., and Brooks, E. A.: Analysis of Experimental Data Regarding Certain Design Features of Pressure Vessels. Trans. ASME, vol. 72, no. 5, July 1950, pp. 567-577.

18. Hardenbergh, Donald E.: Stresses in Contoured Openings of Pressure Vessels. Paper 58-A-207, ASME, 1958.

19. Schoessow, Glen John: Reinforcement of Large Openings in Thin Shells. M. S. Thesis, Purdue Univ., June 1953.

20. Mantle, J. B.: Photoelastic Analysis of Reinforced Stress Raiser. Proc. Soc. Exp. Stress Analysis, vol. 11, no. 2, 1954, pp. 161-172.

21. Kaufman, A., Bizon, P. T., and Morgan, W. C.: Investigation of Tapered Circular Ring Reinforcements around Circular Holes in Flat Sheets Under Biaxial Loads in the Elastic Range. NASA TN D-1101, 1961.

TABLE I. - THEORETICAL AND EXPERIMENTAL EFFECTIVE STRESS-CONCENTRATION FACTORS

X	Z	Stress-field ratio	Experimental stress-concentration factor				Theoretical stress-concentration factor				
			K_C	K_V	K_H	K_O	K_C	K_V	K_H	K_O at Θ_{exp}	$K_{O,max}$
1	1	1:1	1.96	----	----	----	2.000	-----	-----	-----	-----
		1.5:1	2.58	----	----	----	2.646	-----	-----	-----	-----
		2:1	2.80	----	----	----	2.886	-----	-----	-----	-----
		2.5:1	2.89	----	----	----	2.983	-----	-----	-----	-----
1.4	3	1:1	1.26	1.02	1.00	1.04	1.204	1.020	1.020	1.020	1.020
		1.5:1	1.67	.87	1.05	1.10	1.630	.865	1.054	1.144	1.152
		2:1	1.83	.75	1.04	1.19	1.795	.747	1.021	1.290	1.297
		2.5:1	1.89	.67	1.01	1.24	1.863	.657	.933	1.389	1.394
	5	1:1	1.30	0.98	0.94	0.99	0.861	1.004	1.004	1.004	1.004
		1.5:1	1.60	.87	.97	1.05	1.207	.907	.992	1.167	1.168
		2:1	1.71	.78	.94	1.14	1.347	.805	.885	1.352	1.354
		2.5:1	1.75	.71	.91	1.20	1.408	.730	.886	1.475	1.476
	7	1:1	1.36	0.96	0.92	0.99	0.670	1.033	1.033	1.033	1.033
		1.5:1	1.59	.86	.93	1.04	.972	.931	1.004	1.202	1.203
		2:1	1.66	.77	.91	1.12	1.098	.856	.938	1.397	1.397
		2.5:1	1.68	.71	.88	1.18	1.155	.784	.881	1.524	1.525
	9	1:1	1.33	0.95	0.91	0.99	0.549	1.064	1.064	1.064	1.064
		1.5:1	1.52	.86	.92	1.03	.821	.983	1.024	1.232	1.232
		2:1	1.57	.78	.89	1.10	.937	.899	.951	1.426	1.426
		2.5:1	1.58	.73	.86	1.16	.991	.829	.891	1.553	1.553
	11	1:1	1.32	0.98	0.93	1.00	0.464	1.091	1.091	1.091	1.091
		1.5:1	1.50	.90	.94	1.04	.715	1.022	1.042	1.254	1.254
		2:1	1.55	.82	.90	1.11	.824	.935	.984	1.444	1.444
		2.5:1	1.55	.77	.87	1.16	.876	.866	.900	1.567	1.569
1.7	3	1:1	1.01	0.99	0.96	0.95	1.062	1.003	1.003	1.003	1.003
		1.5:1	1.42	.94	.94	1.00	1.477	.946	.952	1.107	1.109
		2:1	1.58	.88	.90	1.08	1.643	.867	.877	1.260	1.264
		2.5:1	1.65	.83	.87	1.13	1.715	.805	.817	1.354	1.359
	5	1:1	0.81	0.97	0.95	0.96	0.723	1.049	1.049	1.049	1.049
		1.5:1	1.10	.99	.88	1.01	1.049	1.035	.947	1.178	1.178
		2:1	1.22	.96	.82	1.08	1.185	.975	.842	1.328	1.328
		2.5:1	1.27	.93	.78	1.13	1.247	.922	.783	1.428	1.429
	7	1:1	0.81	0.99	0.95	0.98	0.548	1.093	1.093	1.093	1.093
		1.5:1	1.02	1.03	.87	1.03	.823	1.099	.986	1.209	1.211
		2:1	1.10	1.02	.80	1.09	.940	1.048	.845	1.362	1.362
		2.5:1	1.13	1.00	.76	1.13	.995	.999	.757	1.459	1.459
	9	1:1	0.87	0.99	0.95	0.96	0.441	1.126	1.126	1.126	1.126
		1.5:1	1.01	1.05	.86	1.01	.681	1.147	.932	1.244	1.247
		2:1	1.06	1.05	.79	1.07	.785	1.102	.860	1.377	1.382
		2.5:1	1.07	1.03	.75	1.11	.834	1.055	.755	1.473	1.473
	11	1:1	0.86	0.98	0.94	0.94	0.369	1.151	1.151	1.151	1.151
		1.5:1	.97	1.05	.85	1.00	.582	1.183	.992	1.259	1.267
		2:1	1.00	1.05	.78	1.05	.676	1.143	.851	1.367	1.393
		2.5:1	1.00	1.04	.74	1.08	.721	1.099	.751	1.473	1.473
2.0	3	1:1	0.95	0.99	1.04	1.08	0.994	1.021	1.021	1.021	1.021
		1.5:1	1.33	1.00	.96	1.13	1.386	1.019	.917	1.120	1.121
		2:1	1.48	.97	.88	1.20	1.543	.970	.816	1.231	1.237
		2.5:1	1.54	.95	.82	1.25	1.611	.924	.742	1.305	1.316
	5	1:1	0.69	1.00	1.06	1.05	0.661	1.083	1.083	1.083	1.083
		1.5:1	.96	1.06	.92	1.11	.956	1.123	.924	1.191	1.191
		2:1	1.06	1.06	.81	1.18	1.079	1.091	.788	1.303	1.304
		2.5:1	1.11	1.04	.74	1.22	1.134	1.052	.692	1.377	1.381
	7	1:1	0.65	0.98	1.05	1.03	0.495	1.127	1.127	1.127	1.127
		1.5:1	.82	1.07	.88	1.09	.735	1.189	.942	1.213	1.216
		2:1	.89	1.08	.77	1.14	.837	1.165	.788	1.339	1.339
		2.5:1	.91	1.07	.70	1.18	.884	1.130	.681	1.409	1.410

TABLE I. - Concluded. THEORETICAL AND EXPERIMENTAL EFFECTIVE STRESS-CONCENTRATION FACTORS

X	Z	Stress-field ratio	Experimental stress-concentration factor				Theoretical stress-concentration factor				
			K_C	K_V	K_H	K_O	K_C	K_V	K_H	K_O at Θ_{exp}	$K_{O,max}$
2.0	9	1:1	0.65	0.96	1.04	1.01	0.396	1.158	1.158	1.158	1.158
		1.5:1	.77	1.06	.86	1.06	.593	1.233	.955	1.260	1.267
		2:1	.81	1.08	.74	1.11	.686	1.215	.790	1.360	1.360
		2.5:1	.83	1.07	.67	1.14	.727	1.183	.676	1.424	1.424
	11	1:1	0.68	0.97	1.03	1.03	0.330	1.179	1.179	1.179	1.179
		1.5:1	.77	1.08	.86	1.07	.506	1.265	.976	1.279	1.290
		2:1	.79	1.11	.74	1.12	.580	1.253	.790	1.372	1.374
		2.5:1	.80	1.11	.67	1.15	.619	1.223	.671	1.433	1.433
2.5	3	1:1	0.93	1.03	1.05	0.99	0.937	1.048	1.048	1.048	1.048
		1.5:1	1.28	1.09	.90	1.12	1.296	1.101	.893	1.136	1.136
		2:1	1.41	1.09	.80	1.21	1.438	1.081	.767	1.215	1.218
		2.5:1	1.47	1.07	.73	1.25	1.499	1.052	.682	1.267	1.275
	5	1:1	0.61	1.03	1.06	0.99	0.612	1.115	1.115	1.115	1.115
		1.5:1	.85	1.13	.87	1.12	.868	1.206	.906	1.214	1.221
		2:1	.95	1.15	.74	1.20	.972	1.199	.743	1.294	1.294
		2.5:1	.99	1.14	.66	1.24	1.019	1.175	.632	1.344	1.346
	7	1:1	0.50	1.05	1.08	0.99	0.454	1.157	1.157	1.157	1.157
		1.5:1	.69	1.17	.87	1.12	.655	1.265	.923	1.257	1.272
		2:1	.76	1.19	.72	1.20	.738	1.265	.743	1.334	1.335
		2.5:1	.79	1.19	.63	1.23	.775	1.243	.622	1.380	1.380
	9	1:1	0.46	1.01	1.05	0.97	0.361	1.184	1.184	1.184	1.202
		1.5:1	.59	1.14	.84	1.10	.527	1.303	.935	1.284	1.306
		2:1	.64	1.17	.69	1.17	.596	1.307	.745	1.357	1.361
		2.5:1	.66	1.16	.61	1.20	.627	1.287	.617	1.400	1.401
	11	1:1	0.45	1.00	1.05	0.95	0.300	1.202	1.202	1.202	1.202
		1.5:1	.55	1.13	.82	1.07	.441	1.329	.943	1.302	1.330
		2:1	.58	1.15	.68	1.13	.498	1.337	.777	1.373	1.380
		2.5:1	.59	1.15	.59	1.16	.527	1.318	.615	1.415	1.415
3.0	3	1:1	0.89	1.00	0.98	1.08	0.909	1.065	1.065	1.065	1.065
		1.5:1	1.20	1.09	.84	1.17	1.245	1.148	.882	1.158	1.158
		2:1	1.32	1.10	.74	1.21	1.377	1.144	.744	1.215	1.217
		2.5:1	1.37	1.09	.68	1.23	1.433	1.124	.654	1.249	1.259
	5	1:1	0.56	1.03	1.01	1.09	0.588	1.133	1.133	1.133	1.133
		1.5:1	.77	1.15	.81	1.19	.820	1.248	.898	1.239	1.250
		2:1	.85	1.17	.68	1.24	.914	1.255	.722	1.301	1.301
		2.5:1	.89	1.16	.60	1.26	.954	1.238	.606	1.335	1.337
	7	1:1	0.42	1.05	1.04	1.14	0.435	1.172	1.172	1.172	1.172
		1.5:1	.58	1.19	.82	1.24	.613	1.302	.915	1.282	-----
		2:1	.64	1.22	.67	1.29	.685	1.314	.723	1.344	1.345
		2.5:1	.66	1.22	.58	1.30	.717	1.298	.596	1.376	1.376
	9	1:1	0.34	1.02	1.07	1.12	0.345	1.197	1.197	1.197	1.197
		1.5:1	.45	1.17	.83	1.22	.490	1.336	.927	1.309	-----
		2:1	.50	1.20	.67	1.25	.549	1.345	.727	1.369	1.373
		2.5:1	.52	1.20	.57	1.27	.575	1.335	.593	1.400	1.400
	11	1:1	0.32	1.02	1.06	1.11	0.286	1.213	1.213	1.213	1.213
		1.5:1	.41	1.17	.81	1.22	.408	1.359	.936	1.328	-----
		2:1	.44	1.21	.65	1.26	.458	1.375	.729	1.387	1.393
		2.5:1	.46	1.21	.56	1.28	.481	1.361	.592	1.416	1.416

TABLE II. - MAXIMUM EFFECTIVE STRESS-CONCENTRATION FACTORS

X	Z	Stress-field ratio	θ for $K_{exp,max}$	θ for $K_{tn,max}$	$K_{exp,max}$	K_{tn} at θ_{exp}	$K_{tn,max}$
1.4	3	1:1	C	C	1.20	.204	1.204
		1.5:1	↓	↓	1.67	.630	1.630
		2:1			1.35	.736	1.736
		2.5:1			1.48	.563	1.483
	5	1:1	C	In sheet	1.30	.861	1.004
		1.5:1	↓	↓	1.61	.207	1.207
		2:1		46.12°	1.71	.347	1.364
		2.5:1		46.15°	1.77	.408	1.476
	7	1:1	C	In sheet	1.38	.670	1.033
		1.5:1		48.82°	1.65	.972	1.303
		2:1		48.92°	1.68	.098	1.397
		2.5:1		48.91°	1.68	.195	1.825
	9	1:1	C	In sheet	1.33	.549	1.064
		1.5:1		48.98°	1.52	.821	1.232
		2:1		49.60°	1.67	.837	1.426
		2.5:1		49.40°	1.65	.891	1.853
	11	1:1	C	In sheet	1.32	.464	1.091
		1.5:1		48.55°	1.50	.715	1.264
		2:1		48.33°	1.62	.824	1.444
		2.5:1		48.26°	1.68	.876	1.969
1.7	3	1:1	C	C	1.01	.062	1.062
		1.5:1	↓	↓	1.42	.477	1.477
		2:1			1.58	.843	1.843
		2.5:1			1.68	.715	1.715
	5	1:1	In sheet	In sheet	0.96	.049	1.049
		1.5:1	C	41.88°	1.10	.049	1.178
		2:1	↓	43.14°	1.22	.155	1.328
		2.5:1		43.05°	1.27	.247	1.429
	7	1:1	In sheet	In sheet	0.97	.033	1.093
		1.5:1	0°	38.56°	1.03	.039	1.071
		2:1	C	42.07°	1.10	.340	1.562
		2.5:1	42°	42.72°	1.13	.439	1.489
	9	1:1	In sheet	In sheet	0.99	.126	1.126
		1.5:1	0°	38.80°	1.08	.147	1.247
		2:1	42°	41.14°	1.07	.377	1.382
		2.5:1	42°	42.03°	1.11	.473	1.473
	11	1:1	In sheet	In sheet	0.96	.191	1.151
		1.5:1	0°	37.18°	1.08	.183	1.267
		2:1	0°	40.34°	1.06	.143	1.383
		2.5:1	42°	41.39°	1.08	.473	1.479
2.0	3	1:1	In sheet	In sheet	1.04	.021	1.021
		1.5:1	C	C	1.33	.386	1.386
		2:1	↓	↓	1.48	.643	1.643
		2.5:1			1.54	.611	1.611
	5	1:1	In sheet	In sheet	1.04	.083	1.083
		1.5:1	38°	38.02°	1.11	.191	1.191
		2:1		39.67°	1.16	.303	1.304
		2.5:1	↓	40.86°	1.22	.377	1.381

X	Z	Stress-field ratio	θ for $K_{exp,max}$	θ for $K_{tn,max}$	$K_{exp,max}$	K_{tn} at θ_{exp}	$K_{tn,max}$
2.0	7	1:1	In sheet	In sheet	1.02	1.127	1.127
		1.5:1	0°	41.07°	1.08	1.218	1.218
		2:1	↓	38.00°	1.14	1.334	1.334
		2.5:1		39.05°	1.18	1.408	1.410
	9	1:1	In sheet	In sheet	1.00	1.186	1.186
		1.5:1	38°	36.60°	1.06	1.260	1.267
		2:1	↓	36.80°	1.11	1.380	1.380
		2.5:1		38.80°	1.14	1.424	1.424
	11	1:1	In sheet	In sheet	1.01	1.173	1.179
		1.5:1	0°	28.32°	1.08	1.265	1.030
		2:1	38°	38.34°	1.12	1.372	1.374
		2.5:1	38°	37.55°	1.15	1.433	1.433
2.5	3	1:1	In sheet	In sheet	1.02	1.044	1.048
		1.5:1	0°	0°	1.28	1.286	1.286
		2:1	↓	↓	1.41	1.436	1.438
		2.5:1			1.47	1.489	1.499
	5	1:1	In sheet	In sheet	1.03	1.115	1.115
		1.5:1	0°	28.33°	1.14	1.206	1.221
		2:1	34.0°	34.12°	1.20	1.284	1.284
		2.5:1	34.5°	36.62°	1.24	1.344	1.346
	7	1:1	In sheet	In sheet	1.04	1.187	1.187
		1.5:1	0°	21.18°	1.17	1.265	1.272
		2:1	34.5°	31.84°	1.20	1.334	1.335
		2.5:1	34.5°	34.91°	1.23	1.380	1.380
	9	1:1	In sheet	In sheet	1.01	1.202	1.202
		1.5:1	0°	16.42°	1.14	1.321	1.306
		2:1	34.5°	30.01°	1.17	1.303	1.361
		2.5:1	34.5°	33.56°	1.21	1.400	1.401
	11	1:1	In sheet	In sheet	1.00	1.202	1.202
		1.5:1	0°	12.31°	1.13	1.329	1.330
		2:1	0°	26.47°	1.16	1.337	1.360
		2.5:1	34.5°	32.04°	1.18	1.411	1.411
3.0	3	1:1	In sheet	In sheet	1.02	1.060	1.060
		1.5:1	0°	0°	1.20	1.244	1.244
		2:1	↓	↓	1.32	1.376	1.377
		2.5:1			1.37	1.433	1.433
	5	1:1	In sheet	In sheet	1.04	1.133	1.133
		1.5:1	30°	21.04°	1.16	1.239	1.250
		2:1	↓	28.36°	1.24	1.301	1.301
		2.5:1		33.03°	1.26	1.338	1.337
	7	1:1	In sheet	In sheet	1.08	1.172	1.172
		1.5:1	30°	4.65°	1.24	1.282	1.309
		2:1		26.04°	1.29	1.344	1.345
		2.5:1	↓	31.30°	1.30	1.376	1.376
	9	1:1	In sheet	In sheet	1.07	1.187	1.187
		1.5:1	30°	0°	1.22	1.309	1.330
		2:1		24.93°	1.25	1.360	1.373
		2.5:1	↓	29.96°	1.27	1.400	1.400
	11	1:1	In sheet	In sheet	1.08	1.213	1.213
		1.5:1	30°	0°	1.22	1.329	1.330
		2:1		23.37°	1.28	1.387	1.393
		2.5:1	↓	28.90°	1.29	1.414	1.416

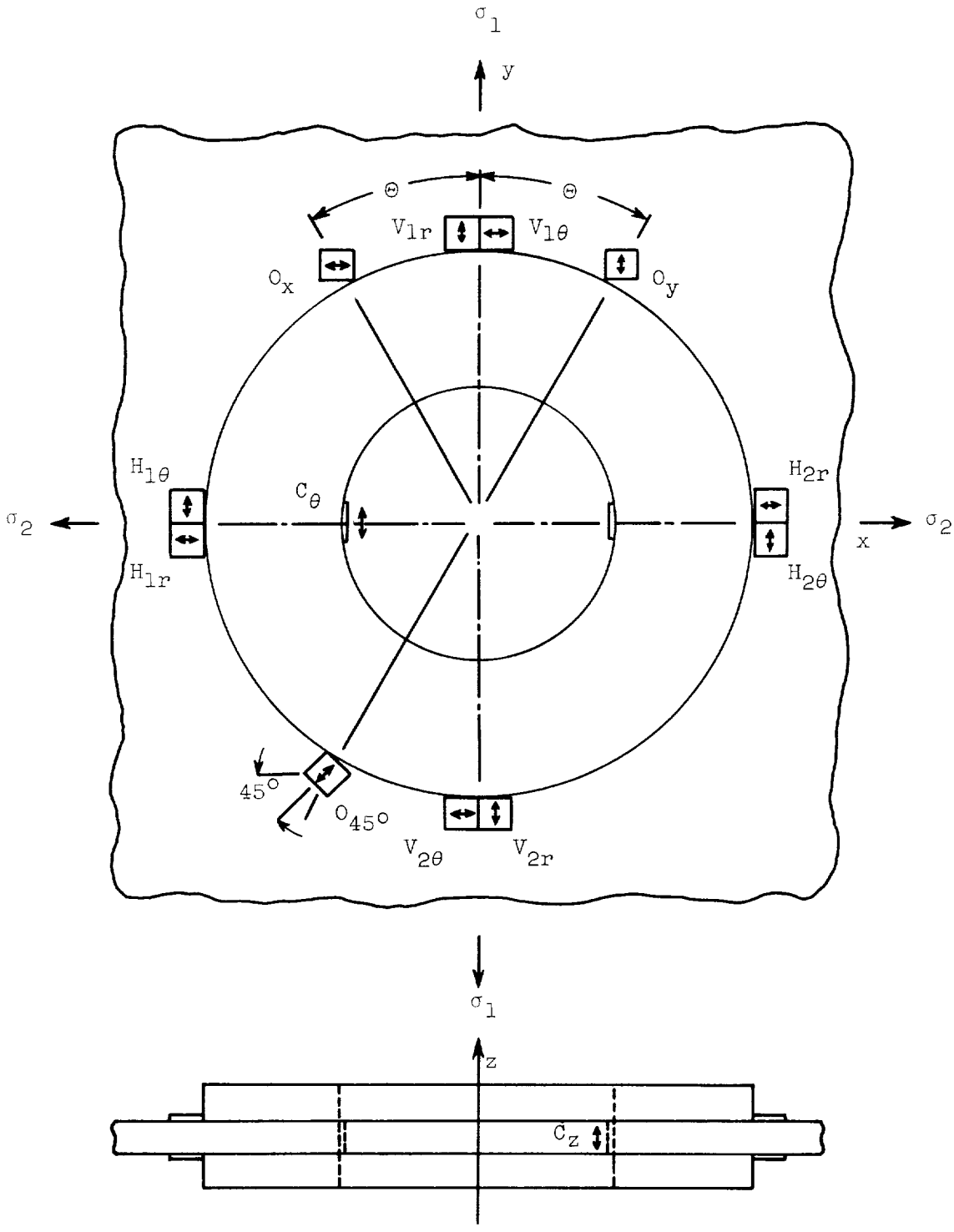

Figure 1. - Location and orientation of strain gages in reinforcement area of specimen.

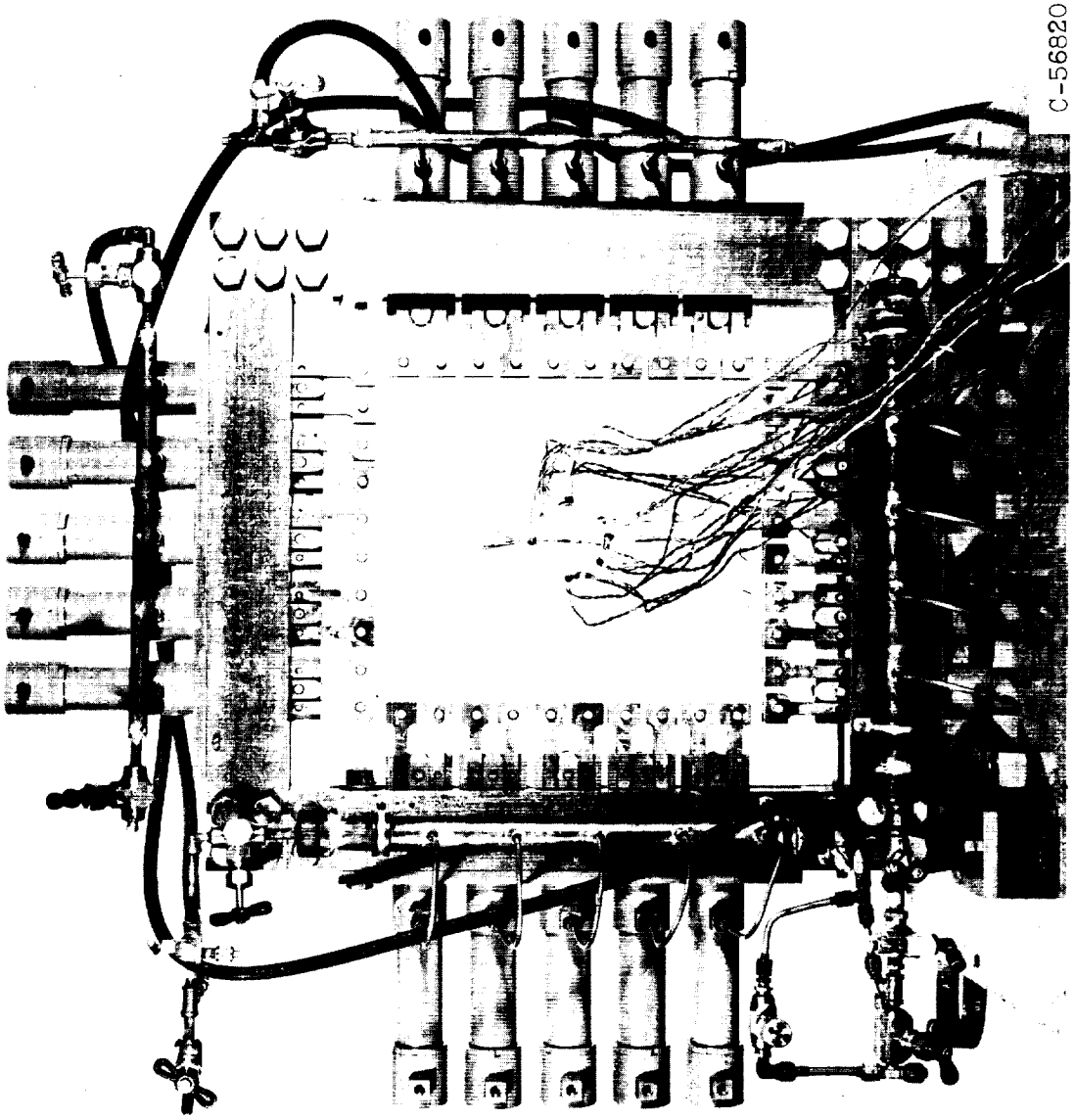

C-56820

Figure 2. - Biaxial tensile machine.

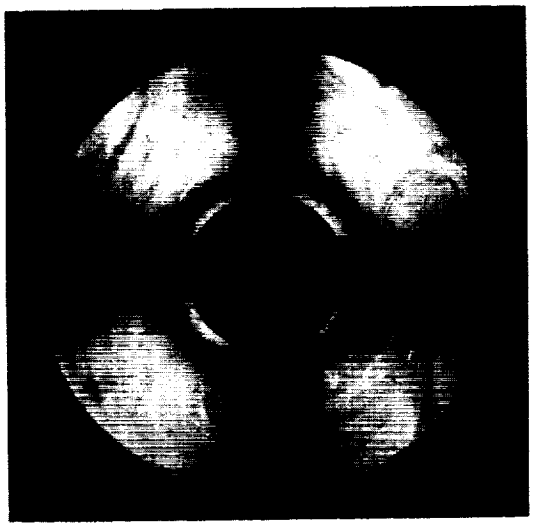

(a) Stress-field ratio, 1:1.

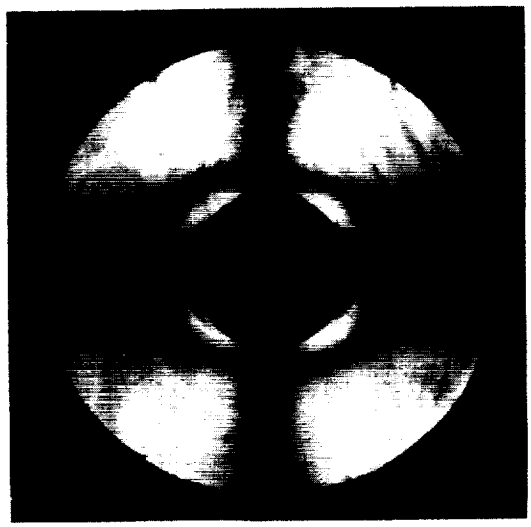

(b) Stress-field ratio, 1.5:1.

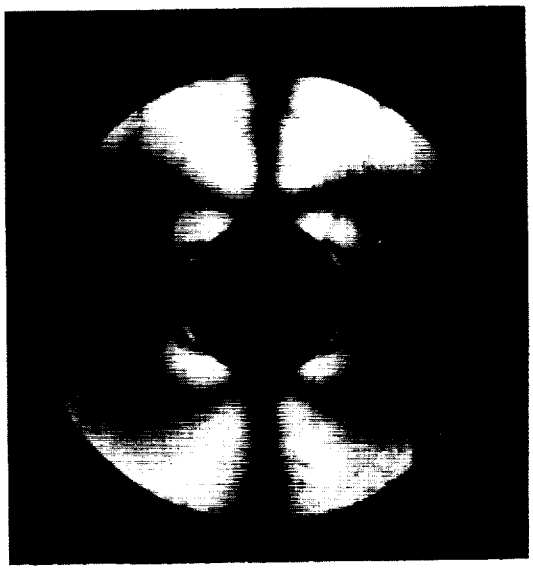

(c) Stress-field ratio, 2:1.

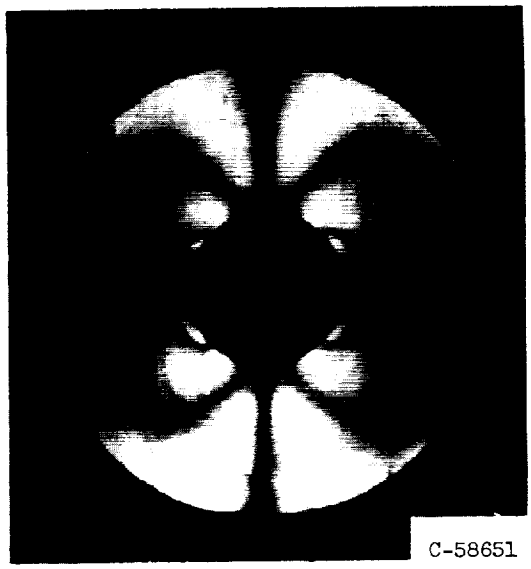

(d) Stress-field ratio, 2.5:1.

Figure 3. - Photoelastic patterns. Hub diameter ratio X, 3; hub-sheet thickness ratio Z, 3.

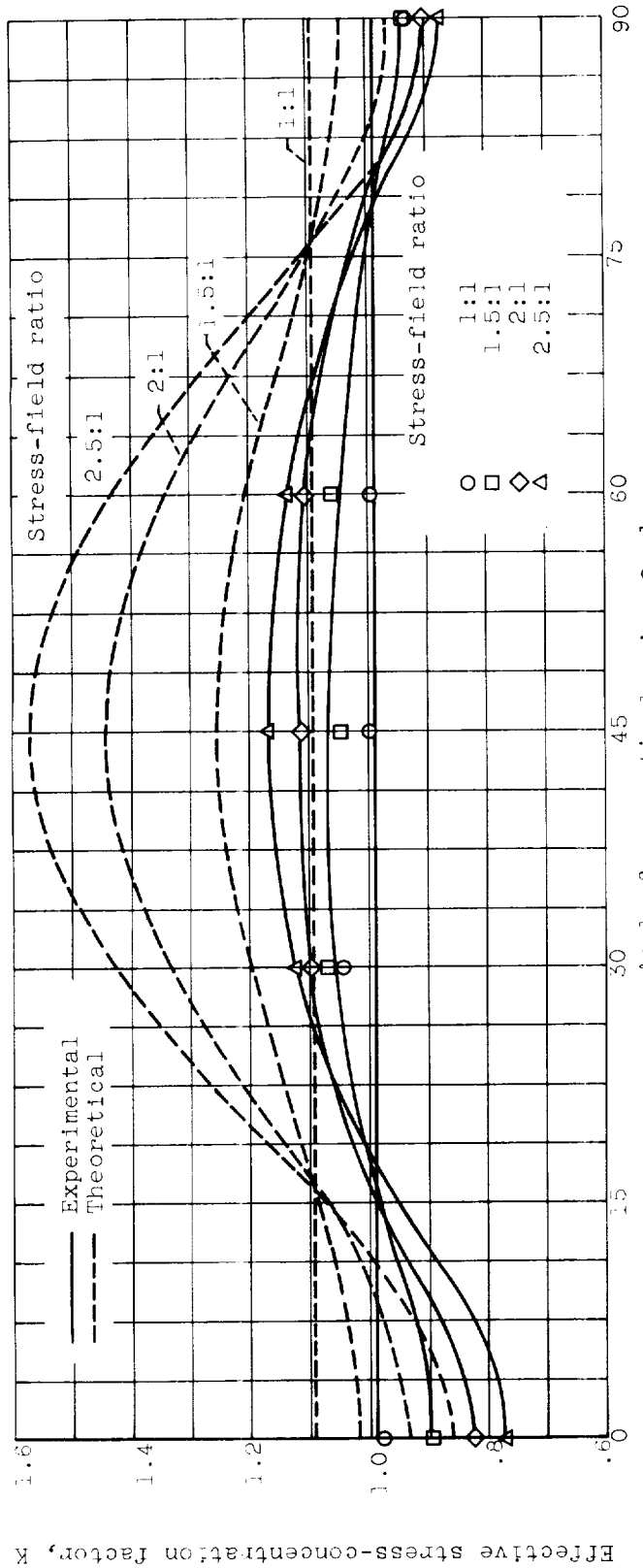

Figure 4. - Comparison of theoretical and experimental effective stress-concentration factors in sheet. Hub diameter ratio X, 1.4; hub-sheet thickness ratio Z, 11.

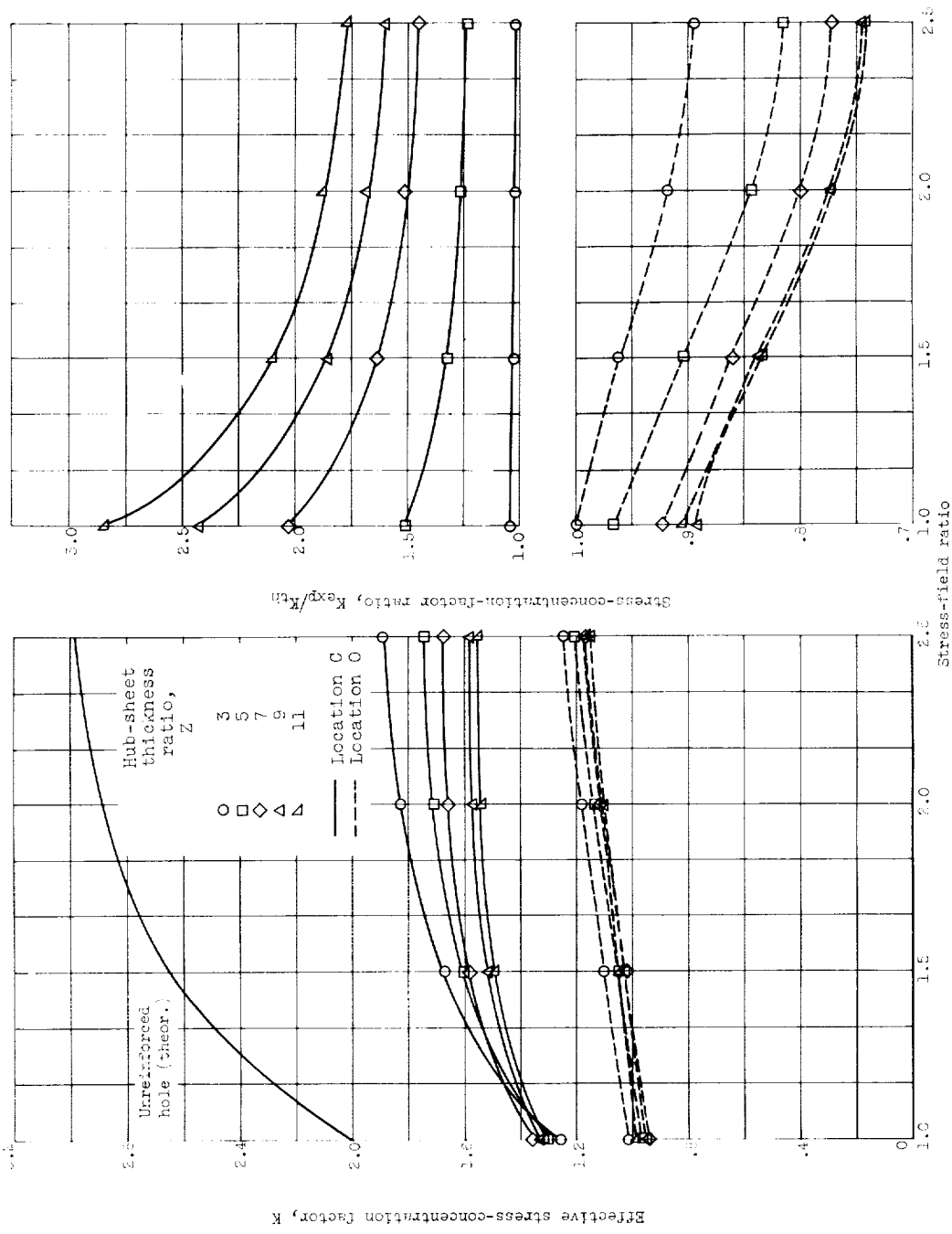

(a) H.b diameter ratio X, 1.4.

Figure 3. - Effect of stress-field ratio on stress-concentration factor and comparison with theoretical predictions.

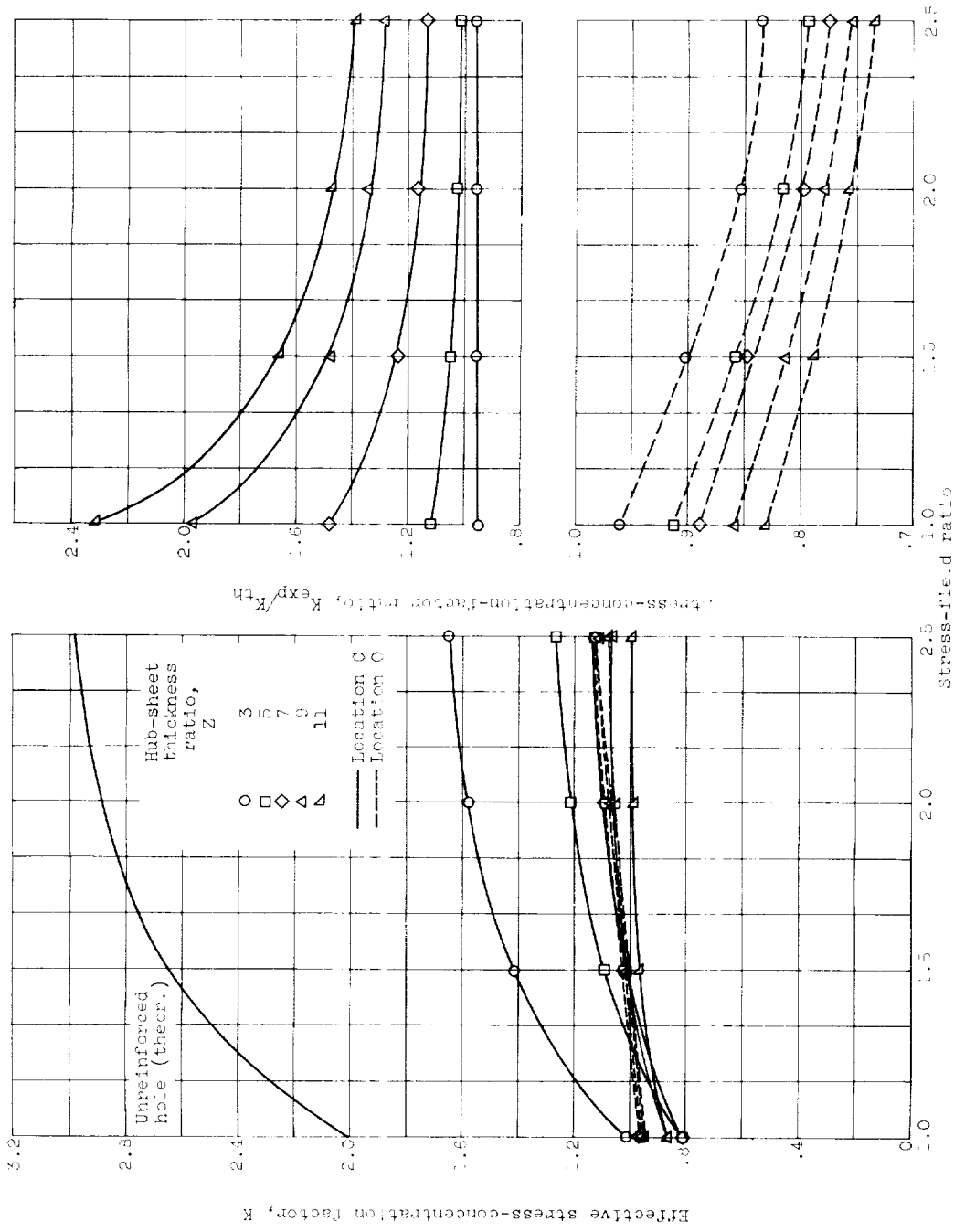

(b) Hub diameter ratio X, 1.7.

Figure 5. - Continued. Effect of stress-field ratio on stress-concentration factor and comparison with theoretical predictions.

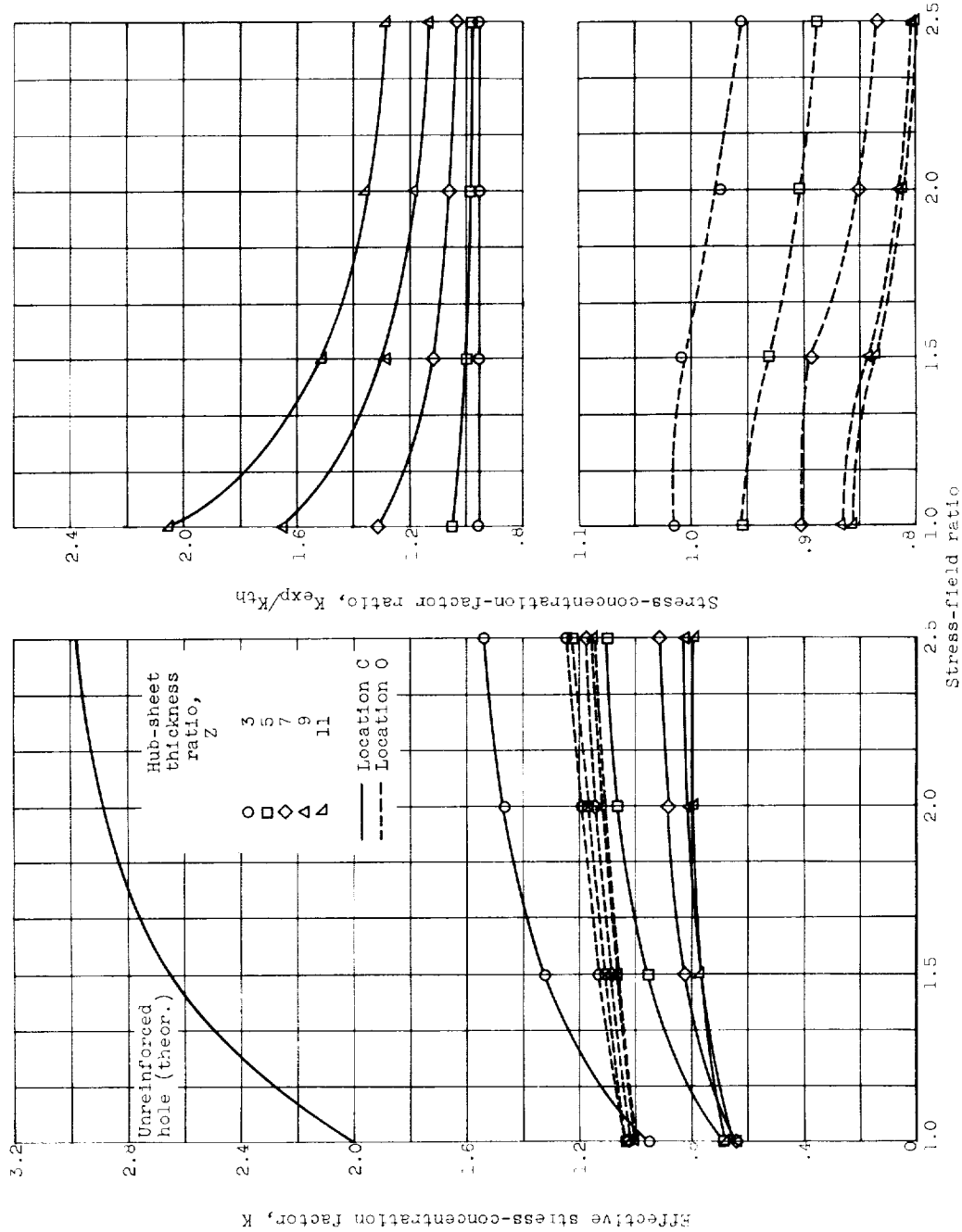

(c) Hub diameter ratio X, 2.0.

Figure 3. - Continued. Effect of stress-field ratio on stress-concentration factor and comparison with theoretical predictions.

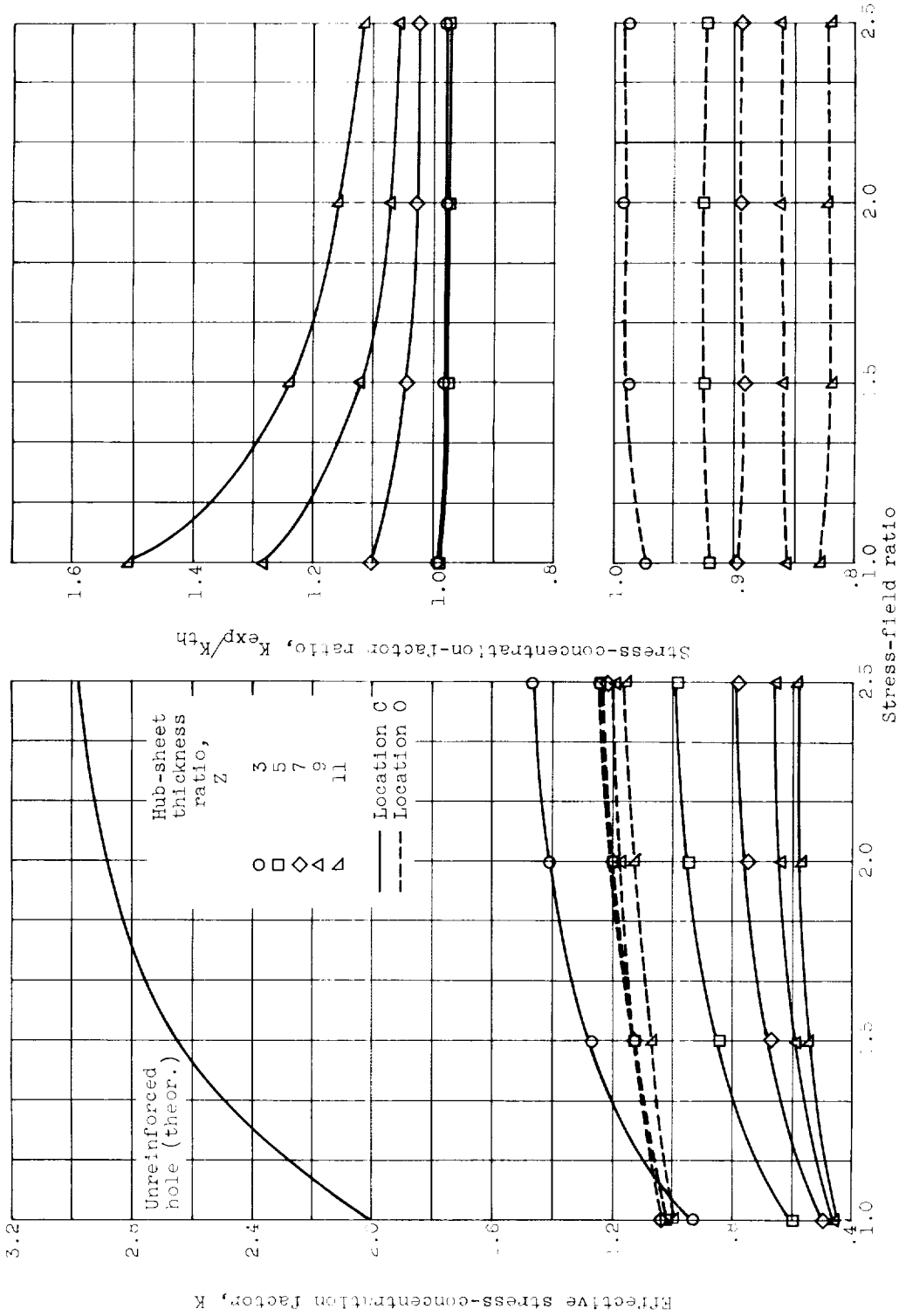

(d) Hub diameter ratio X, 2.5.

Figure 5. - Continued. Effect of stress-field ratio on stress-concentration factor and comparison with theoretical predictions.

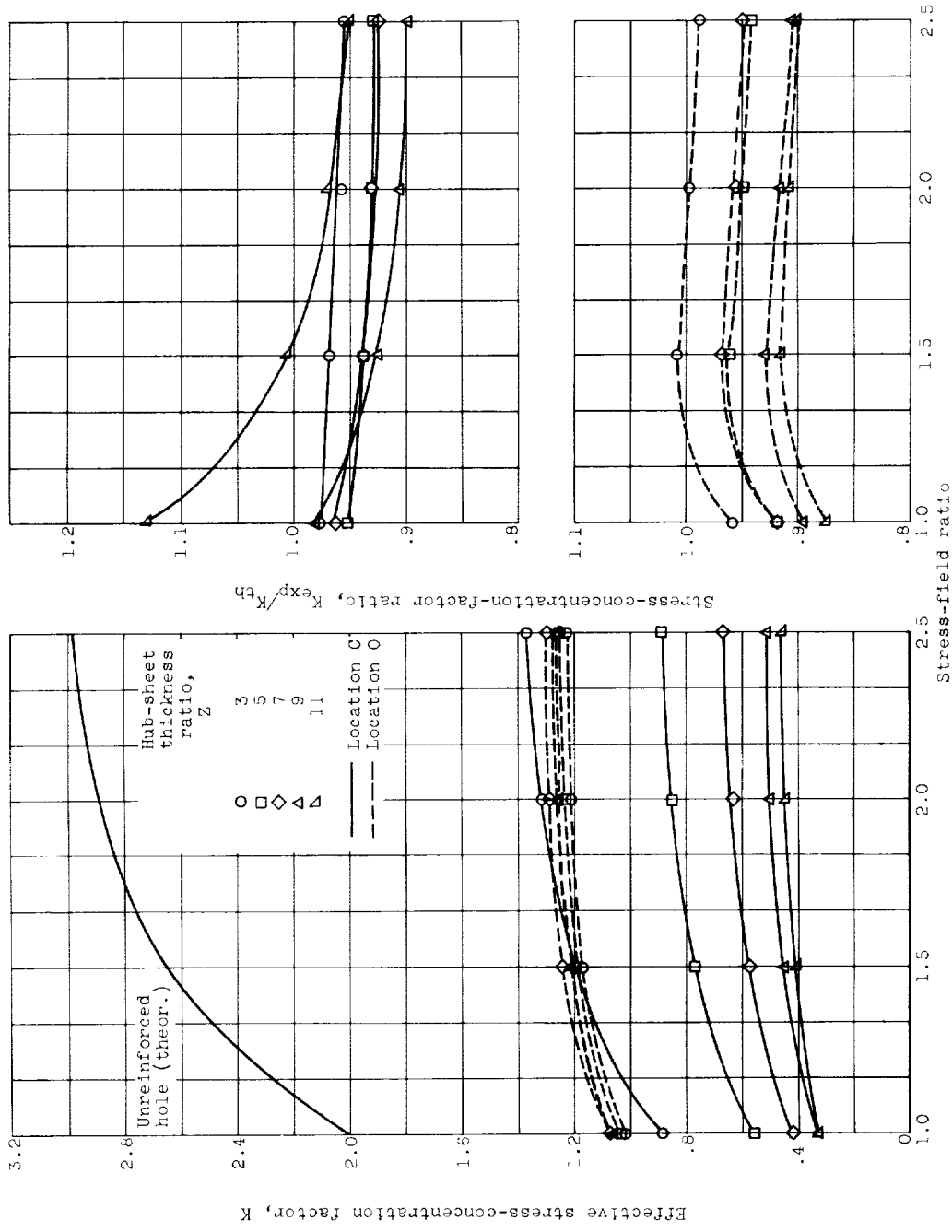

(e) Hub diameter ratio X, 3.0.

Figure 5. - Concluded. Effect of stress-field ratio on stress-concentration factor and comparison with theoretical predictions.

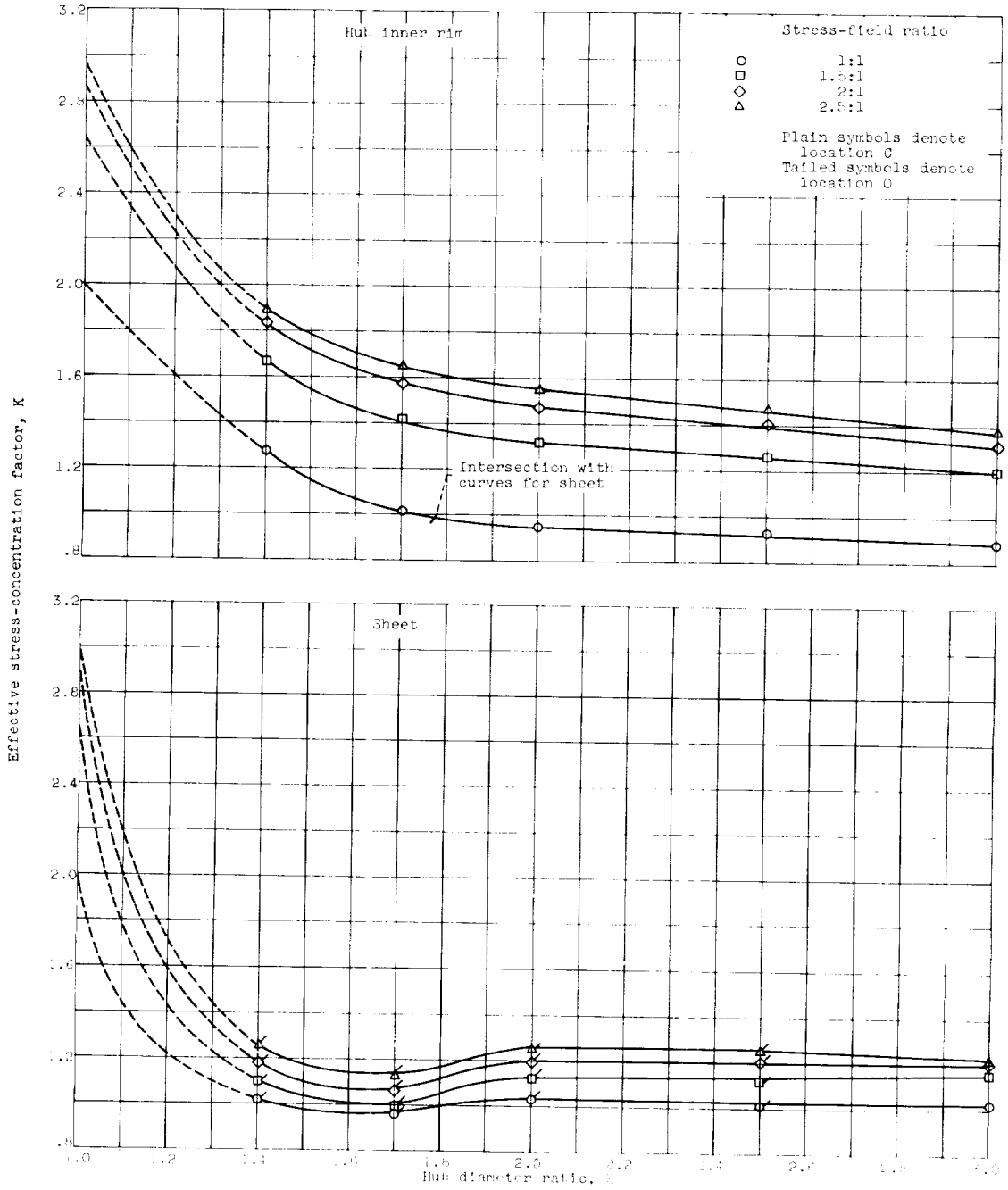

(a) Hub-sheet thickness ratio t_h/t_s.

Figure 6. - Effect of hub diameter on maximum stress concentration.

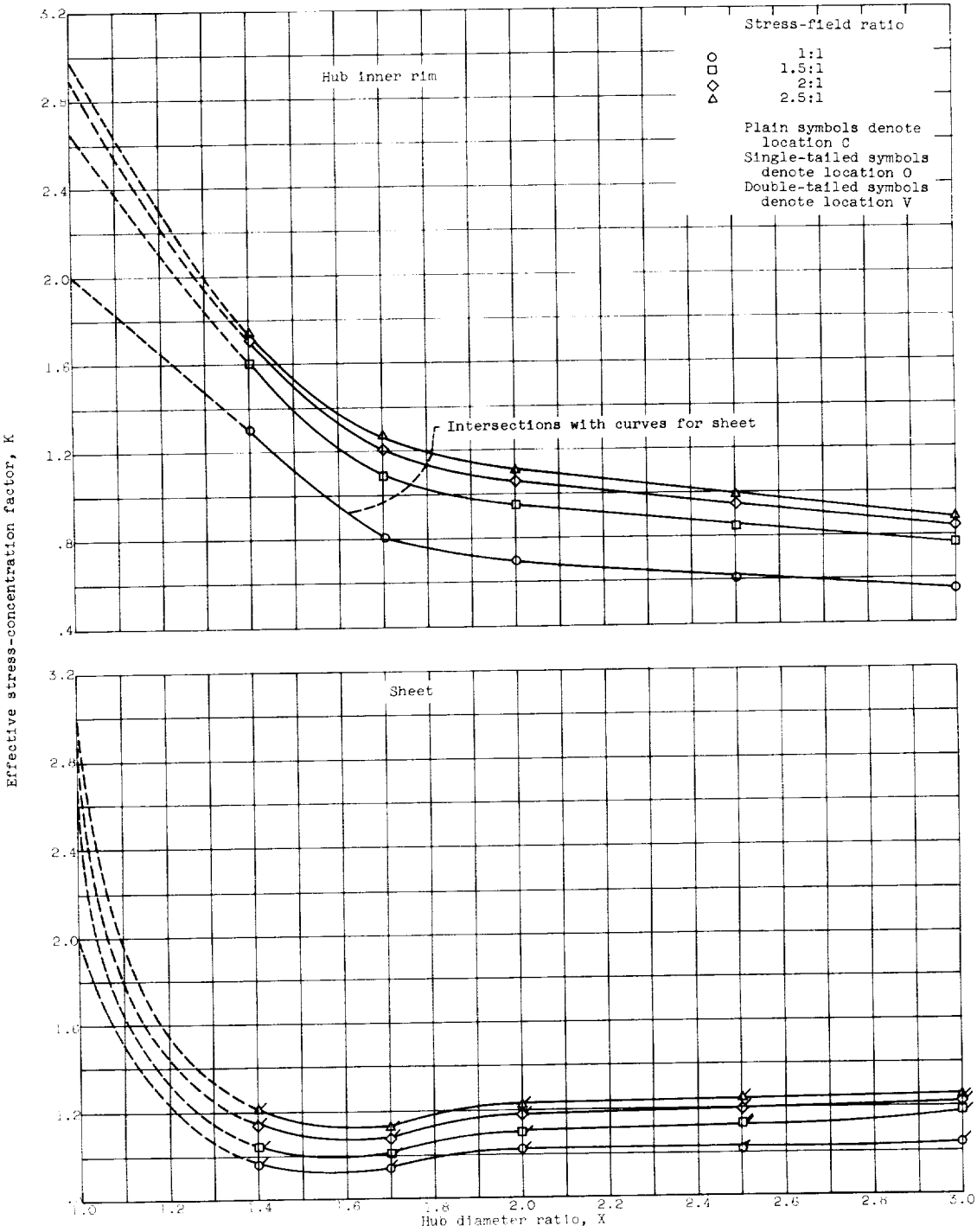

(b) Hub-sheet thickness ratio Z, 5.

Figure 6. - Continued. Effect of hub diameter on maximum stress concentration.

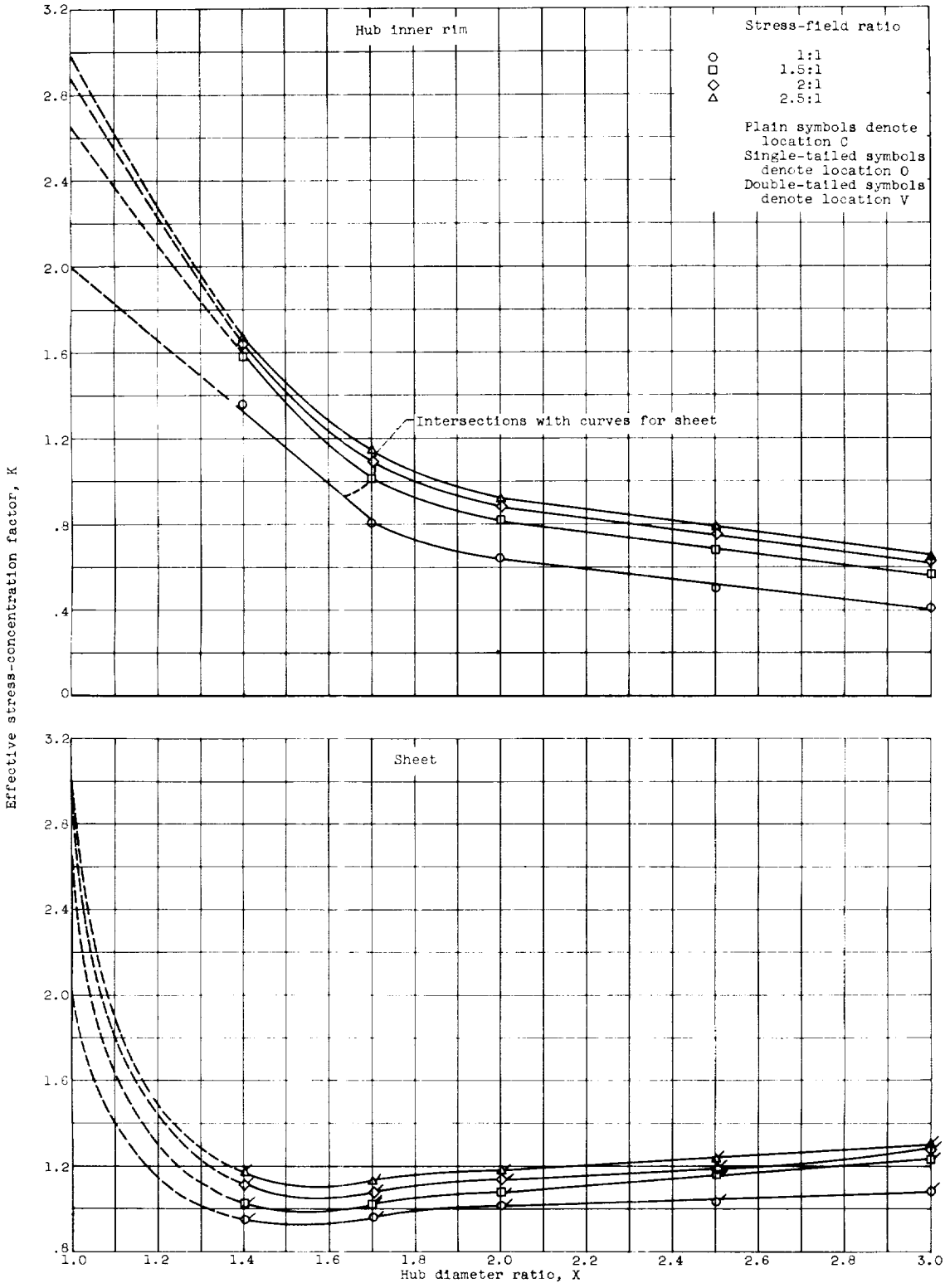

(c) Hub-sheet thickness ratio Z, 7.

Figure 6.- Continued. Effect of hub diameter on maximum stress concentration.

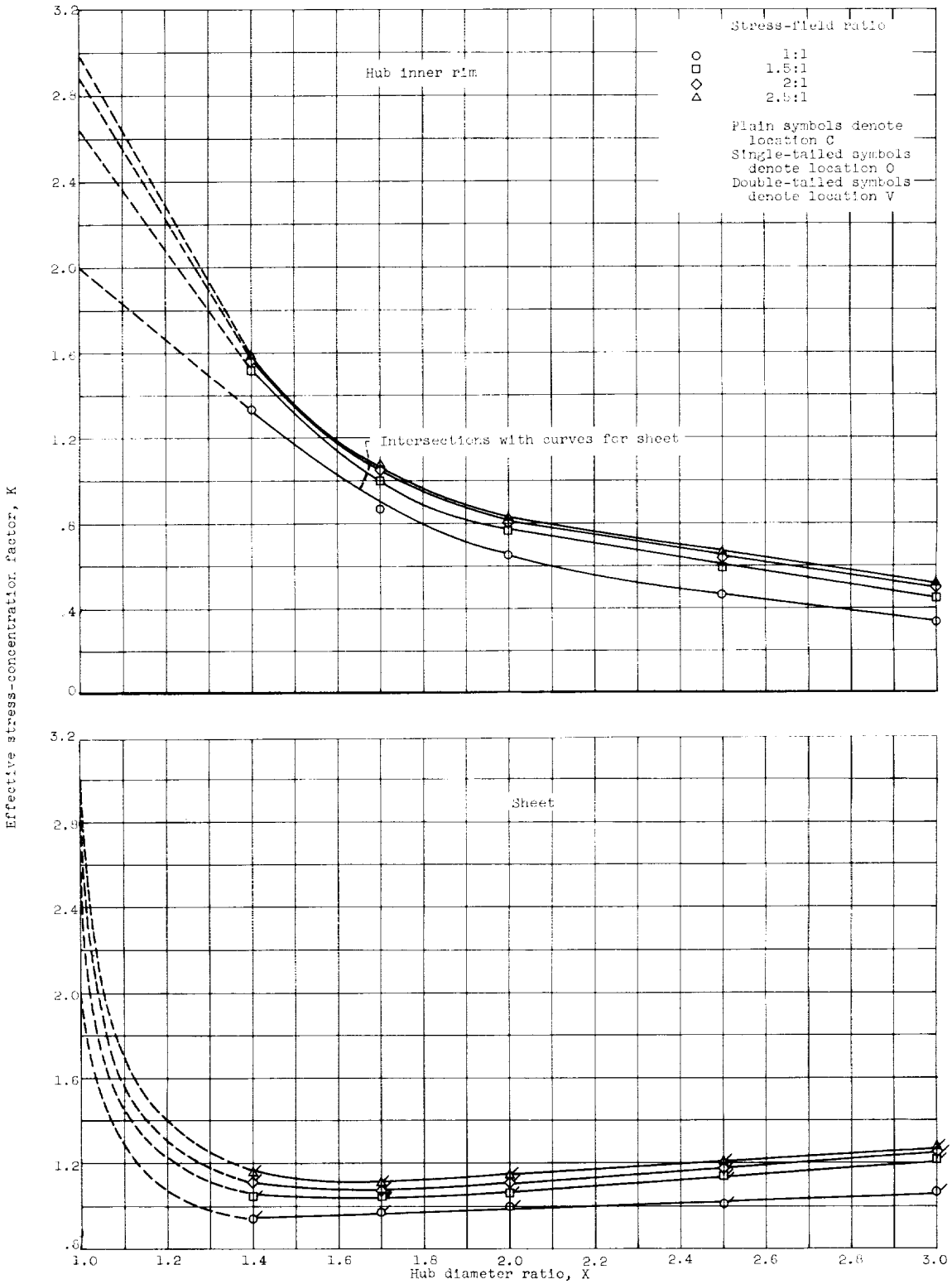

(d) Hub-sheet thickness ratio Z, 9.

Figure 6. - Continued. Effect of hub diameter on maximum stress concentration.

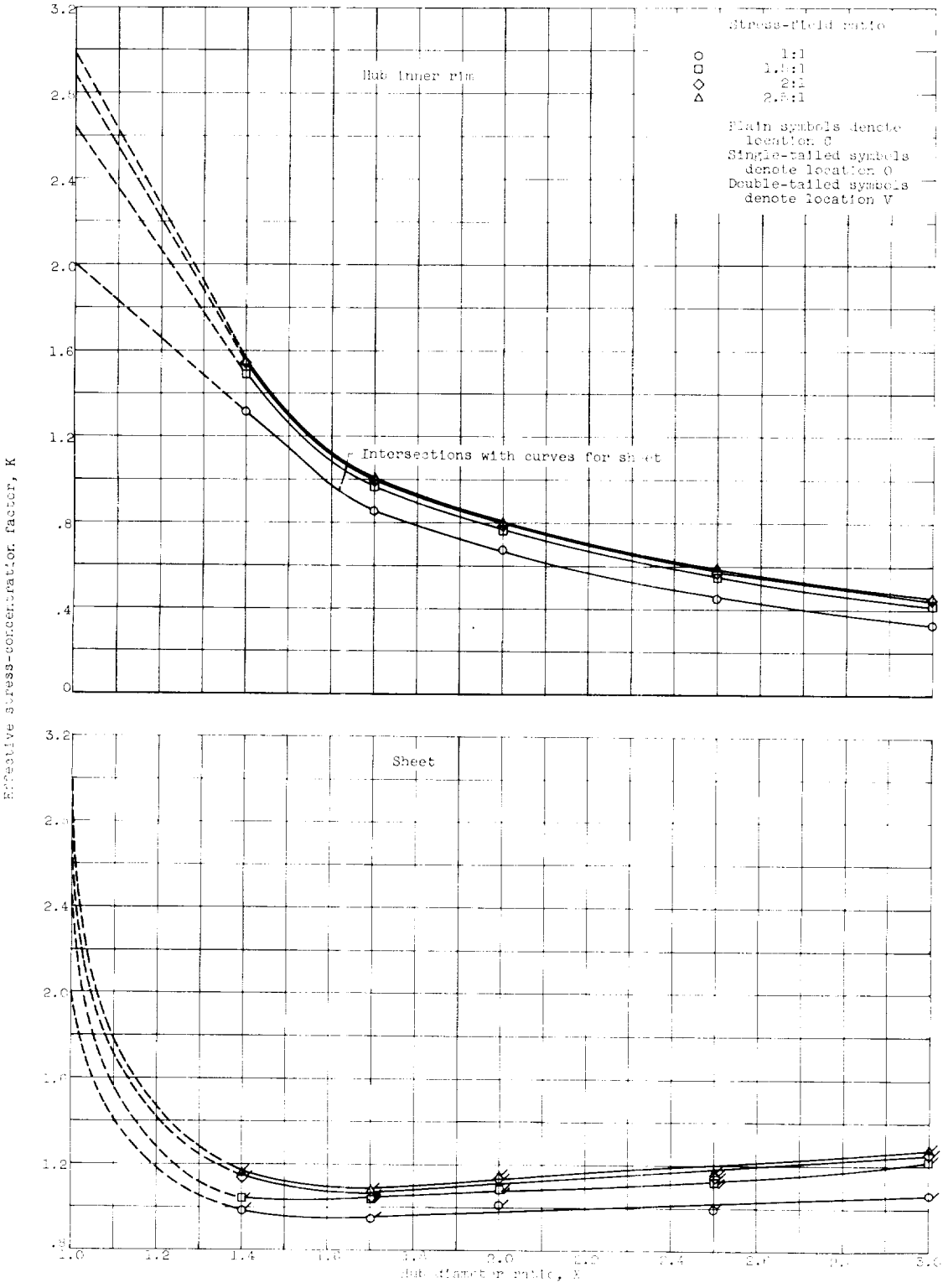

(a) Hub-sheet thickness ratio 2, D/t.

Figure 6. - Concluded. Effect of hub diameter on maximum stress concentration.

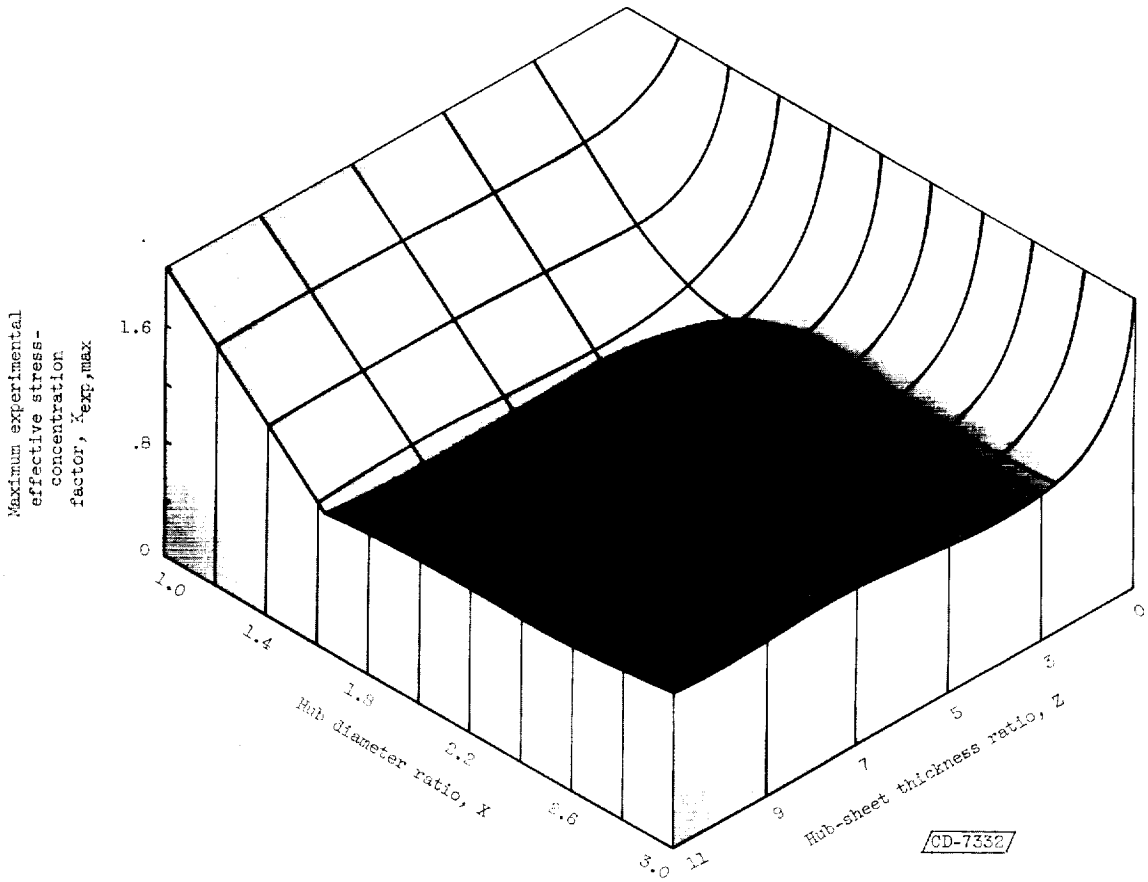

(a) Stress-field ratio, 1:1.

Figure 7. - Maximum experimental effective stress-concentration factor plotted against hub diameter ratio and hub-sheet thickness ratio.

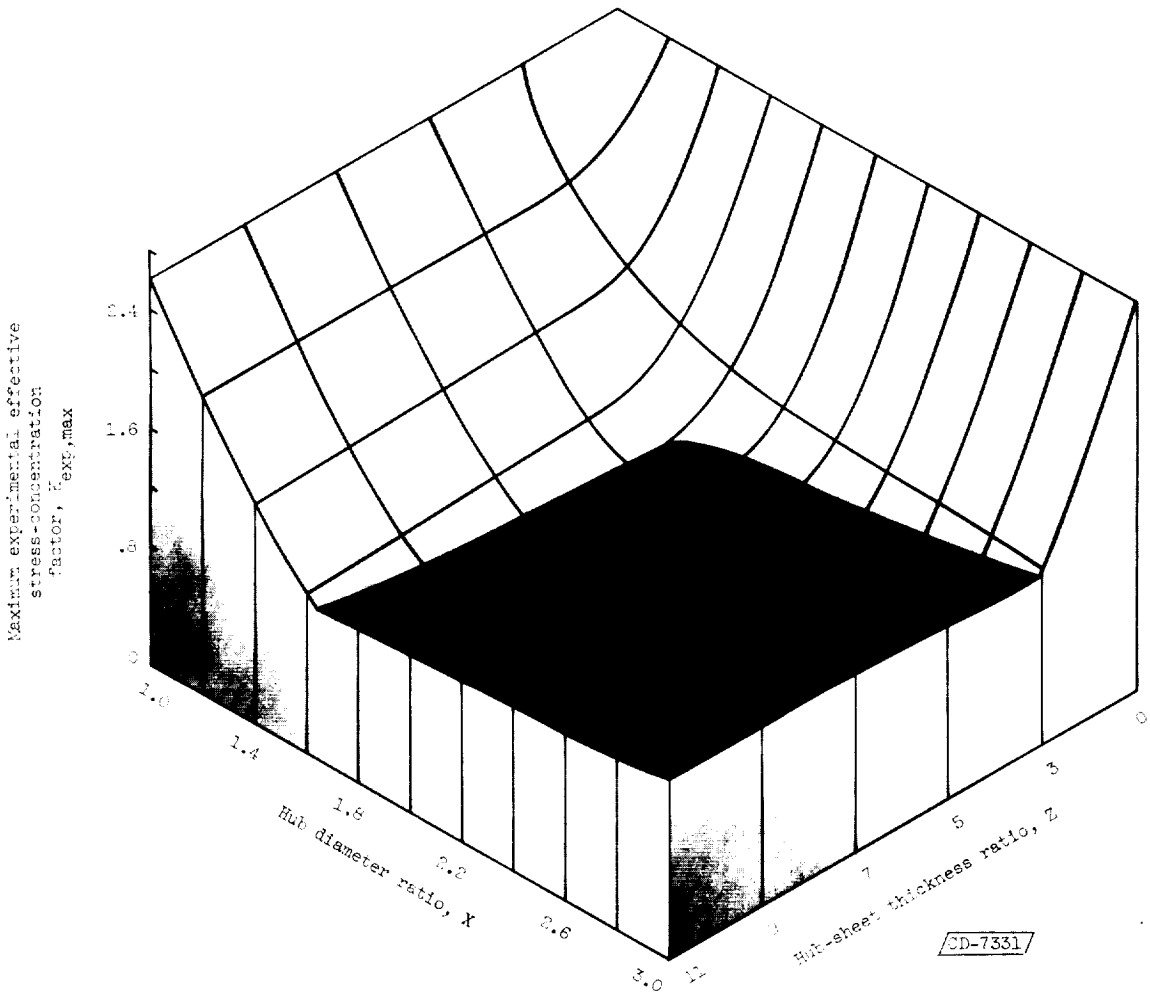

(b) Stress-field ratio, 1.5:1.

Figure 7. - Continued. Maximum experimental effective stress-concentration factor plotted against hub diameter ratio and hub-sheet thickness ratio.

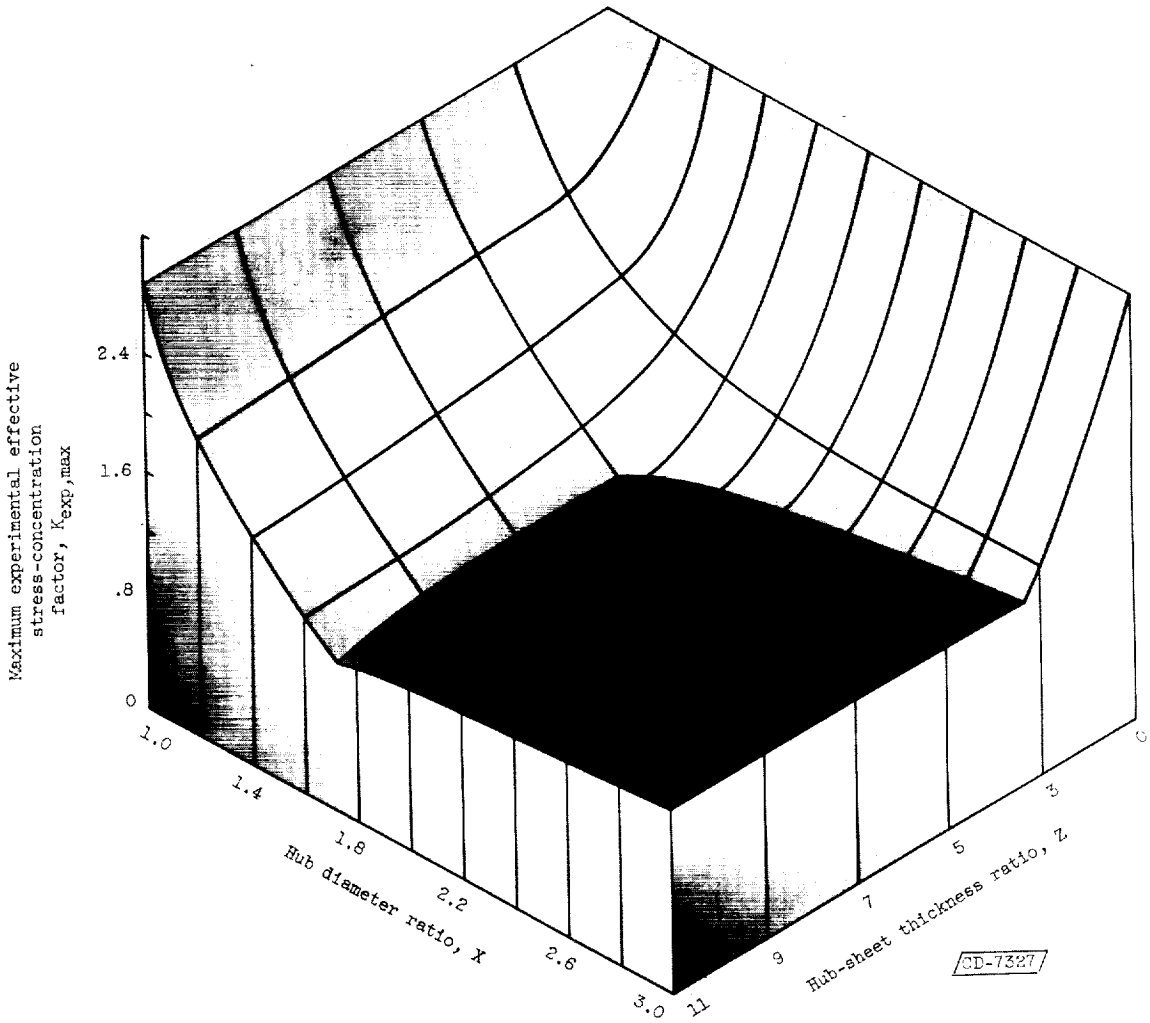

(c) Stress-field ratio, 2:1.

Figure 7. - Continued. Maximum experimental effective stress-concentration factor plotted against hub diameter ratio and hub-sheet thickness ratio.

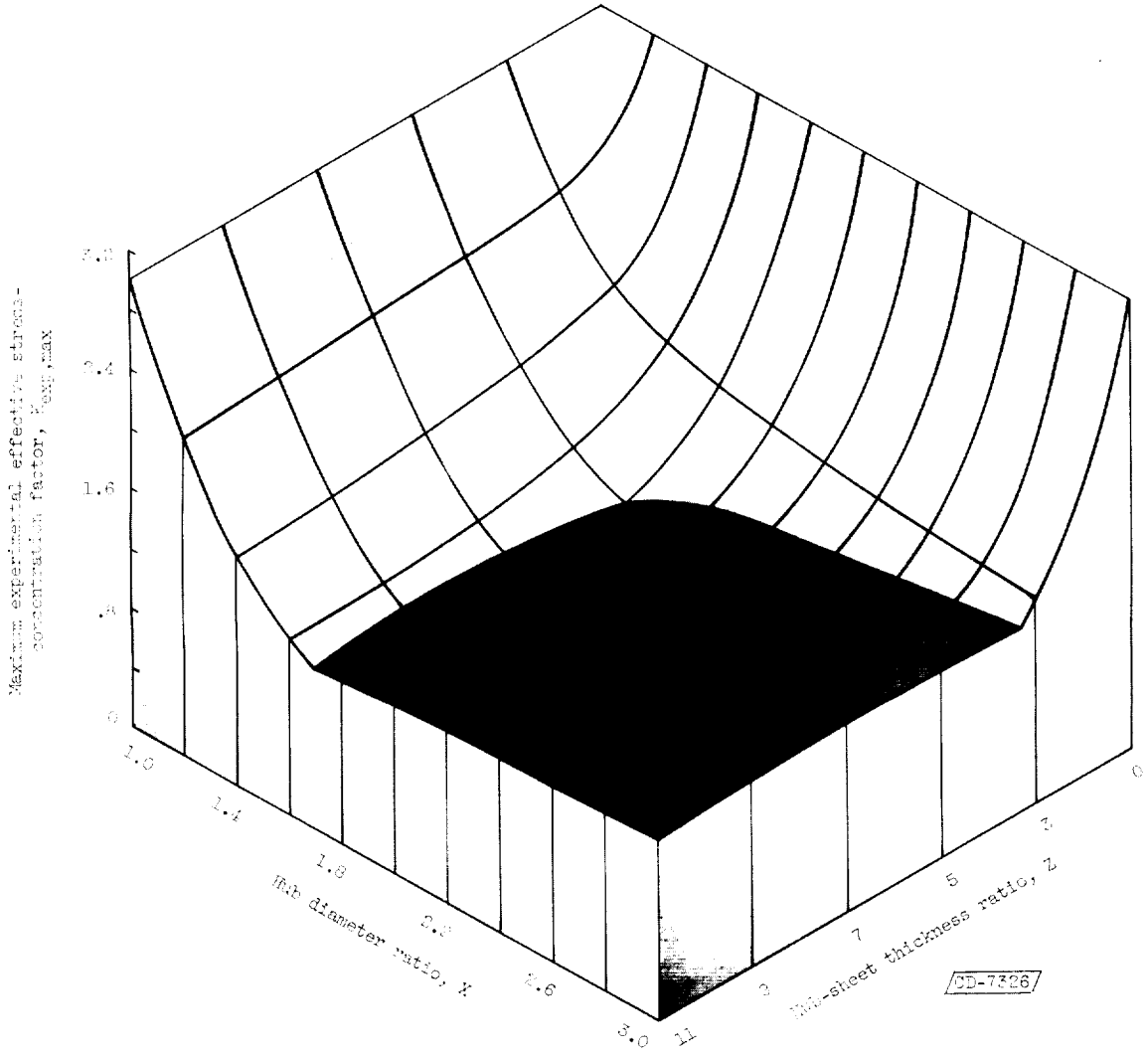

(d) Stress-field ratio, 2.5:1.

Figure 7. - Concluded. Maximum experimental effective stress-concentration factor plotted against hub diameter ratio and hub-sheet thickness ratio.

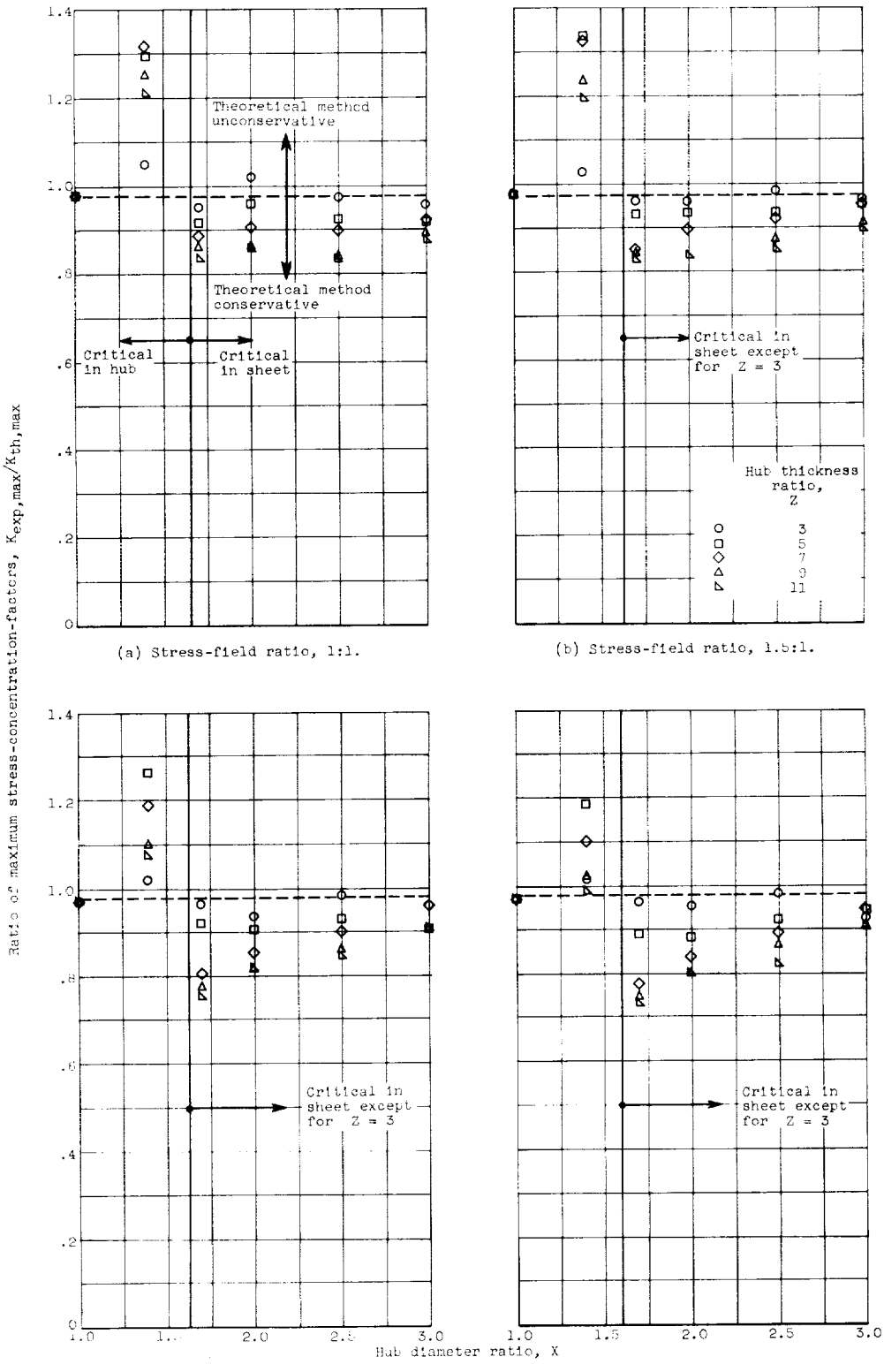

Figure 8. - Comparison of experimental and theoretical maximum effective stress-concentration factors.

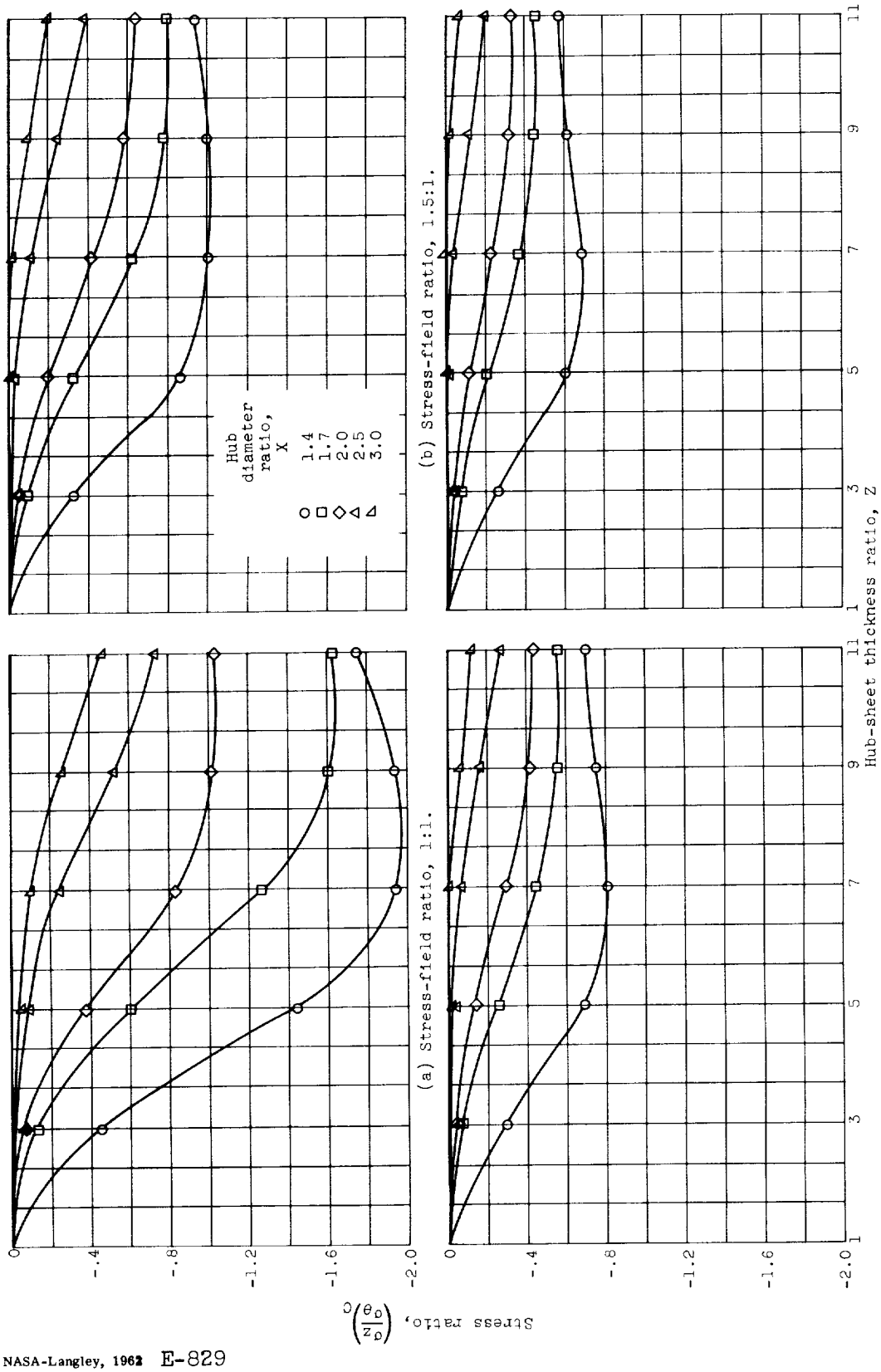

Figure 9. - Effect of geometry of reinforcement on bending stresses.